Geochemistry Geophysics Geosystems G3

Article
Volume 12, Number 7
1 July 2011
Q07002, doi:10.1029/2011GC003616
ISSN: 1525-2027

Published by AGU and the Geochemical Society

New Late Permian paleomagnetic data from Argentina: Refinement of the apparent polar wander path of Gondwana

Mathew Domeier
Department of Geological Sciences, University of Michigan, Ann Arbor, Michigan 48109-1005, USA (domeier@umich.edu)

Rob Van der Voo
Department of Geological Sciences, University of Michigan, Ann Arbor, Michigan 48109-1005, USA (voo@umich.edu)

Also at Center for Advanced Study, Norwegian Academy of Science and Letters, Drammensveien 78, N-0271 Oslo, Norway

Eric Tohver
School of Earth and Geographical Sciences, University of Western Australia, 35 Stirling Highway, Crawley, Western Australia 6009, Australia (etohver@cyllene.uwa.edu.au)

Renata N. Tomezzoli and Haroldo Vizan
Departamento de Ciencias Geológicas, Universidad de Buenos Aires, Pabellón 2, Ciudad Universitaria, C.P. 1428, Buenos Aires, Argentina (renata@gl.fcen.uba.ar; haroldo@gl.fcen.uba.ar)

Trond H. Torsvik
Center for Advanced Study, Norwegian Academy of Science and Letters, Drammensveien 78, N-0271 Oslo, Norway

Also at Department of Physics, University of Oslo, Postboks 1048 Blindern, N-0316 Oslo, Norway (t.h.torsvik@geo.uio.no)

Also at School of Geosciences, University of the Witwatersrand, Wits, Johannesburg, 2050 South Africa

Jordan Kirshner
Department of Geological Sciences, University of Michigan, Ann Arbor, Michigan 48109-1005, USA (jordan.r.kirshner@gmail.com)

[1] The Late Paleozoic–Early Mesozoic apparent polar wander path of Gondwana is largely constructed from relatively old paleomagnetic results, many of which are considered unreliable by modern standards. Paleomagnetic results derived from sedimentary sequences, which are generally poorly dated and prone to inclination shallowing, are especially common. Here we report the results of a joint paleomagnetic-geochronologic study of a volcanic complex in central Argentina. U-Pb dating of zircons has yielded a robust age estimate of 263.0 +1.6/−2.0 Ma for the complex. Paleomagnetic analysis has revealed a pretilting (primary Permian) magnetization with dual polarities. Rock magnetic experiments have identified pseudo-single domain (titano)magnetite and hematite as the mineralogic carriers of the magnetization. Lightning-induced isothermal remagnetizations are widespread in the low-coercivity magnetic carriers. The resulting paleomagnetic pole is 80.1°S, 349.0°E, A_{95} = 3.3°, N = 35, and it improves a Late Permian mean pole calculated from a filtered South American paleomagnetic data set. More broadly, this new, high-quality, igneous-based

paleomagnetic pole falls between the previously distinct Late Permian segments of the Laurussian and Gondwanan apparent polar wander paths, suggesting that the long-recognized disparity between these large paleomagnetic data sets may be primarily due to the inclusion of low-quality or systemically biased data.

Components: 13,400 words, 10 figures, 3 tables.

Keywords: Gondwana; Permian; paleomagnetism.

Index Terms: 1525 Geomagnetism and Paleomagnetism: Paleomagnetism applied to tectonics: regional, global.

Received 7 March 2011; **Revised** 26 April 2011; **Accepted** 27 April 2011; **Published** 1 July 2011.

Domeier, M., R. Van der Voo, E. Tohver, R. N. Tomezzoli, H. Vizan, T. H. Torsvik, and J. Kirshner (2011), New Late Permian paleomagnetic data from Argentina: Refinement of the apparent polar wander path of Gondwana, *Geochem. Geophys. Geosyst.*, *12*, Q07002, doi:10.1029/2011GC003616.

1. Introduction

[2] The Late Paleozoic–Early Mesozoic apparent polar wander path (APWP) for Gondwana is poorly defined, being largely constructed from vintage paleomagnetic results, many of which are derived from sedimentary units which may suffer from known magnetic recording biases (inclination shallowing). Recent paleomagnetic work in western-central Argentina has begun to address the paucity of reliable results, by focusing on a belt of Late Paleozoic–Early Mesozoic volcano-plutonic complexes [*Terrizzano*, 2005; *Tomezzoli et al.*, 2008; *Domeier et al.*, 2009]. However, the published data are mostly preliminary, necessitating additional work to reinforce and validate these initial studies. Continued paleomagnetic and geochronologic work along this belt also has the potential to answer questions about the nature and timing of volcanism and deformation in southwestern Gondwana during the Late Paleozoic. These questions remain critical to understanding the paleogeographic and geologic evolution of this paleomargin [see, e.g., *Tomezzoli*, 2001].

[3] Here we present new results from a continued investigation of volcanic rocks at the Sierra Chica, La Pampa, Argentina. This complex was elected for further study because preliminary paleomagnetic results (10 sites) suggested that a stable, Late Paleozoic magnetization could be isolated, Middle Triassic isotopic age data conflict with an inferred Early Permian (Kiaman) age of magnetization, and structural restorations, applied to only two of the 10 sites in the preliminary study, did not allow a rigorous tilt test to be conducted [*Tomezzoli et al.*, 2008]. Additional sites were collected to evaluate and augment the existing paleomagnetic data set and U-Pb dating was carried out to better define the age of these rocks.

2. Geologic Setting

[4] The Sierra Chica is one of a series of local topographic highs, formed by a resistant sequence of silicic volcanic rocks, located in La Pampa province, Argentina (Figure 1). Together these high elements delineate a discontinuous NW-SE trending belt of Late Paleozoic–Early Mesozoic volcano-plutonic complexes that are considered to be generally correlative with the larger, more continuous belt of the Choiyoi Group, a chain of intermediate to silicic volcanic and shallow plutonic rocks that runs from the San Rafael Block in Mendoza province, Argentina, to the High Andes of northern-central Chile [*Kay et al.*, 1989; *Sruoga and Llambías*, 1992; *Llambías et al.*, 1993; *Llambías et al.*, 2003]. The Choiyoi Group displays an evolving geochemistry that suggests a change from arc-related volcanism in the Early Permian to a transitional-intraplate setting in the Late Permian–Triassic [*Mpodozis and Kay*, 1992; *Llambías and Sato*, 1995; *Martin et al.*, 1999; *Heredia et al.*, 2002; *Kleiman and Japas*, 2009]. A temporally protracted and geographically widespread deformation episode, the San Rafael Orogenic Phase (SROP), is associated with this changing geochemistry, and has been variously attributed to terrane accretion, oblique and/or flat slab subduction, and intraplate tectonic adjustments, either from proximal activity or via transmitted stresses [*Lock*, 1980; *Forsythe*, 1982; *Dalziel and Grunow*, 1992; *Visser and Praekelt*, 1998; *Trouw and De Wit*, 1999; *Pankhurst et al.*, 2006; *Ramos*, 2008; *Kleiman and Japas*, 2009]. Evidence of this deformation is pronounced in the Choiyoi Group to

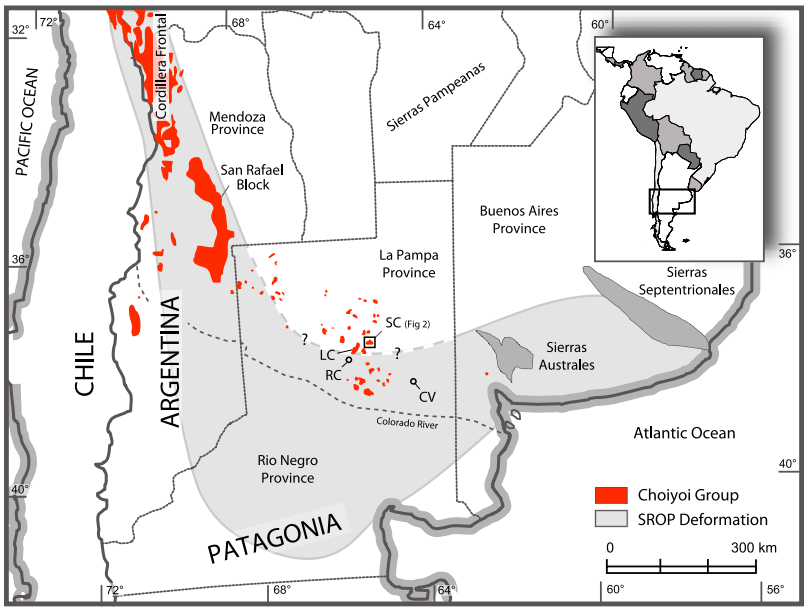

Figure 1. Regional map showing the distribution of Choiyoi Group volcanic rocks and structures associated with the San Rafael Orogenic Phase (SROP) of deformation. Abbreviated place names discussed in the text: CV, Cerro de Los Viejos; LC, Lihue Calel; RC, Rio Curaco; SC, Sierra Chica. The small box in the center of the figure highlights the area illustrated in Figure 2. Adapted from *Tomezzoli et al.* [2008] and *Kleiman and Japas* [2009].

the west of the Sierra Chica, to the east in the fold and thrust belt of the Sierras Australes [*Tomezzoli*, 2001], and to the south in Northern Patagonia (Figure 1). In La Pampa province, however, the effects of this deformation episode are shown only by the gently folded sedimentary rocks of the Permian age Carapacha Basin and by the spatially diminutive Cerro de Los Viejos mylonitic shear belt [*Tickyj et al.*, 1997; *Tomezzoli et al.*, 2006]. This distinction in tectonic setting between the Choiyoi Group proper and volcanic rocks of La Pampa has been recognized geochemically [*Llambías et al.*, 2003].

[5] The Sierra Chica has been subdivided into three distinct petrologic sequences; a lower unit, with a very limited exposure, of trachyandesitic pyroclastic flows, a middle rhyolitic unit comprised of thin (<5 m) pyroclastic flows containing abundant lithic fragments, and interspersed with tuffs, and an upper rhyolitic unit with thick (>5 m) lava flows and ignimbrites exhibiting rheomorphic features (Figure 2) [*Quenardelle and Llambías*, 1997; *Tomezzoli et al.*, 2008]. The changing lithologic character of the mid-to-upper units reflects an evolution of eruptive style, which may be the consequence of a primarily stratified magma chamber with a volatile-rich upper horizon. The thickness and composition of the upper unit suggest that the rocks are proximal to the effusive center, and Sierra Chica itself may be a dissected volcanic edifice [*Llambías*, 1973]. Geochemically, all sequences are identical and exhibit high-K calc-alkaline signatures with metaluminous to slightly peraluminous trends [*Quenardelle and Llambías*, 1997]. The similar structure of the lower and middle units (both dipping ~25°S) is well determined from clearly defined flow horizons and fiamme, whereas the more massive and rheomorphic upper unit rarely yields discernable contacts or consistent fiamme orientation. An average of the measurements from several locations within the upper unit suggests that it is horizontal to very shallowly dipping (≤5°S). *Tomezzoli et al.* [2008] speculated that the lower and middle units may have been tilted by the SROP prior to emplacement of the upper unit.

[6] Assuming that the volcanic rocks of the Sierra Chica and Lihue Calel, a sequence of rhyolitic ignimbrites 15 km to the southwest of the Sierra Chica, are cogenetic, *Rapela et al.* [1996] combined samples from both locations to yield a Rb-Sr whole-rock isochron age estimate of 240 ± 2 Ma. However, differences in structure, stratigraphy, geochemistry, and petrology lend little credence to the premise of a common source for Lihue Calel and the Sierra Chica [*Tomezzoli et al.*, 2008]. Additionally, this age estimate, if valid, only pertains to the lower unit of the Sierra Chica, and can therefore only act as a maximum age for the middle and upper units. Noting an absence of normal polarity magnetic directions,

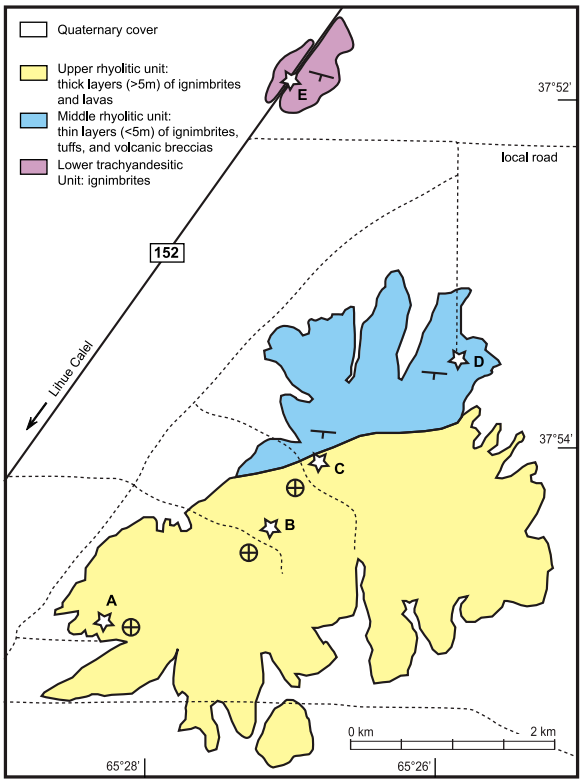

Figure 2. Simplified geologic map of the Sierra Chica showing the three petrologic units and the location of sampling localities (stars). Adapted from *Tomezzoli et al.* [2008].

Tomezzoli et al. [2008] proposed that the volcanic rocks were magnetized during the Kiaman Reversed Superchron (~318–265 Ma [*Opdyke et al.*, 2000; *Gradstein et al.*, 2004]), which would require that the sequence be older than 265 Ma.

3. Methods

[7] Sampling was conducted during two successive field seasons, during which 38 paleomagnetic sites were collected from five principal localities (A–E; Figure 2) distributed along a transect through the stratigraphic section. Localities A and B are in the upper unit, locality C is located at the contact between the upper and middle units, locality D is in the middle unit, and E is in the lower unit. A collection of field-drilled cores (SC collection) was complemented by a collection of hand samples (RS collection). Each site contains a minimum of five independently oriented samples. A solar compass was used to prevent any local magnetic anomalies from affecting orientation readings. Hand samples for isotopic age determinations were collected from each of the three stratigraphic sequences.

[8] Paleomagnetic samples were stored and processed in a magnetically shielded room at the University of Michigan with a residual field of ≤200 nT. Measurements of remanent magnetization were made with a three-axis 2G cryogenic magnetometer. A pilot demagnetization scheme subjected sister specimens to both alternating field (AF) and thermal demagnetization techniques to determine the most effective approach to demagnetization for each site. AF demagnetization was carried out according to a static three-position procedure. Thermal demagnetization was conducted in air; samples were cooled in a magnetically shielded chamber, with a typical DC field of ≤5 nT. Magnetic susceptibility was routinely monitored during pilot thermal demagnetizations to detect any mineralogic changes at high temperatures. Progressive demagnetization was carried out with a minimum of 12 steps, up to 200 mT or 680°C. Demagnetization data were analyzed with orthogonal vector diagrams and stereographic projections [*Zijderveld*, 1967; *Cogné*, 2003]. Principal component analysis was used to quantitatively define magnetization vectors; where persistent and random remagnetizations were observed (i.e., lightning-induced isothermal overprints), converging great circles were used to define the common magnetic direction [*Halls*, 1978; *Kirschvink*, 1980]. *Fisher* [1953] statistics were used to compute site-level mean directions from purely vectorial (stable end point) populations; where remagnetization circles defined some samples, the statistical approach of *McFadden and McElhinny* [1988] was applied.

[9] Rock magnetic experiments were conducted at the Institute for Rock Magnetism in order to identify and characterize the magnetic carriers. Hysteresis measurements and first order reversal curves (FORCs) were generated with a vibrating sample magnetometer operating at room temperature. Low temperature remanence experiments were performed with a magnetic properties measurement system (MPMS); samples were cooled to 20 K in either a field-cooled (FC) or zero-field cooled (ZFC) environment, given an isothermal remanence, and then warmed to room temperature in zero field. Thermomagnetic curves (κ versus T) were measured in an argon atmosphere with a high-temperature susceptibility bridge.

[10] Three samples were collected for analysis using U-Pb SHRIMP geochronology. Zircons were separated by crushing and sieving of samples, followed by Wilfley table and heavy liquid separation. Grains were picked using a binocular microscope and scanning electron microscope (SEM) images of

zircon grains were taken prior to mounting in epoxy resin and polishing for imaging by SEM and cathodoluminescence imaging. Subsequently, SHRIMP analysis was conducted with the SHRIMP II housed at Curtin University. The epoxy mounts were cleaned and gold coated to have a uniform electrical conductivity during the SHRIMP analyses. Samples were measured over two separate analytical sessions, during which the external error calculated from analysis of standards was 0.61% (SC-D01, SC-D03) and 1.4% (SC-D04). The zircon standard used was BR266 zircon (559 Ma, 903ppm U). Prior to spot analysis, rastering of the ion beam was carried out for 120–150 s to remove the gold coating and reduce the common Pb contaminant within the gold coating. A primary ion beam of 2.5–3 nA with a diameter of ~25 μm was focused onto the polished surface. Common Pb corrections were carried out using the measured amount of 204Pb. Isotopic data are reduced using SQUID2 [*Ludwig*, 2003]. Data were plotted on concordia diagrams using Isoplot 3 software [*Ludwig*, 2003], in which error ellipses on concordia plots are shown at the 2σ confidence level. All specific dates reported in the text are U-Pb concordia ages calculated from concordant analyses and include decay constant errors, with age uncertainty reported at the 95% confidence level.

4. Paleomagnetic Results

[11] Sites from locality E, in the lower unit, exhibit very straightforward demagnetization behavior, characterized by a univectorial decay to the origin (Figure 3a); occasionally a very minor overprint is removed in the initial demagnetization steps. All samples from these sites were thermally treated, as a pervasive high-coercivity phase makes AF demagnetization ineffective. The laboratory unblocking temperature spectrum suggests the presence of two phases in sites SC04, SC05, and RS17, as the remanence is principally removed within two discrete intervals separated by a stable plateau. The initial unblocking of remanence generally falls between 550°C and 585°C, whereas the second (terminal) unblocking occurs above 650°C. The minerals that define such behavior are interpreted to be magnetite and hematite, respectively. Directions derived from the linear segments of the different unblocking temperature intervals are not statistically different, thus the decay is truly univectorial. Samples from site SC20 exhibit a strongly 'shouldered' spectrum with a very narrow unblocking temperature interval above 650°C, suggesting it contains only the hematite component. The directions of the characteristic remanent magnetizations (ChRMs) from all four sites at Locality E are WNW and steeply up (Table 1).

[12] Sites from the D locality, from the middle unit of the sequence, yield broadly similar demagnetization behavior characterized by converging great circle trajectories. A randomly oriented, low-coercivity/temperature component (component A) is superimposed on a more stable component (component B) with a direction that is consistently of steep positive inclination. Multiple samples from a given site yield great circle demagnetization trajectories that track from the random direction toward a common intersection point, parallel to the B component that is isolated to varying success (e.g., Figure 3d). Because the components have a strong coercivity distinction, AF demagnetization is the most effective technique for separating them, but thermal demagnetization yields comparable results (Figure 3b). Component A is interpreted to be an overprint, perhaps an isothermal remagnetization acquired due to lightning. This is supported by the random nature of the directions, as well as the observation that the samples/sites with the most pervasive A components are associated with the highest NRM intensities. Samples from site SC12, for example, have NRM intensities 10–1000x greater than those from neighboring sites with similar lithologies, and these samples yield a single, randomly directed component, suggesting they have been completely overprinted. Site SC12 has therefore been discarded. Site RS01 is also rejected because the mean is ill defined due to subparallel great circles resulting from subparallel overprint directions. Samples from SC09 exhibit univectorial demagnetization behavior with corresponding directions that resemble the B component from neighboring sites. However, AF demagnetization demonstrates that these samples contain a low-coercivity fraction, suggesting that they may have escaped partial remagnetization. Expectedly, these samples have some of the lowest NRM intensities at this locality. In most sites, thermal demagnetization demonstrates that the phase carrying component A is unblocked between 300°C and 585°C, and the B component is not unblocked until 600°C, or above. In some instances, the A-carrying phase is removed over two discrete intervals at about 350°C and 550°C, indicating that two distinct mineralogic components may constitute this low-coercivity/temperature fraction (Figure 3c). This phase is interpreted to be titanomagnetite, perhaps occurring as two populations that differ in titanium content, oxygen parameter, or grain size. Hematite is interpreted to be the

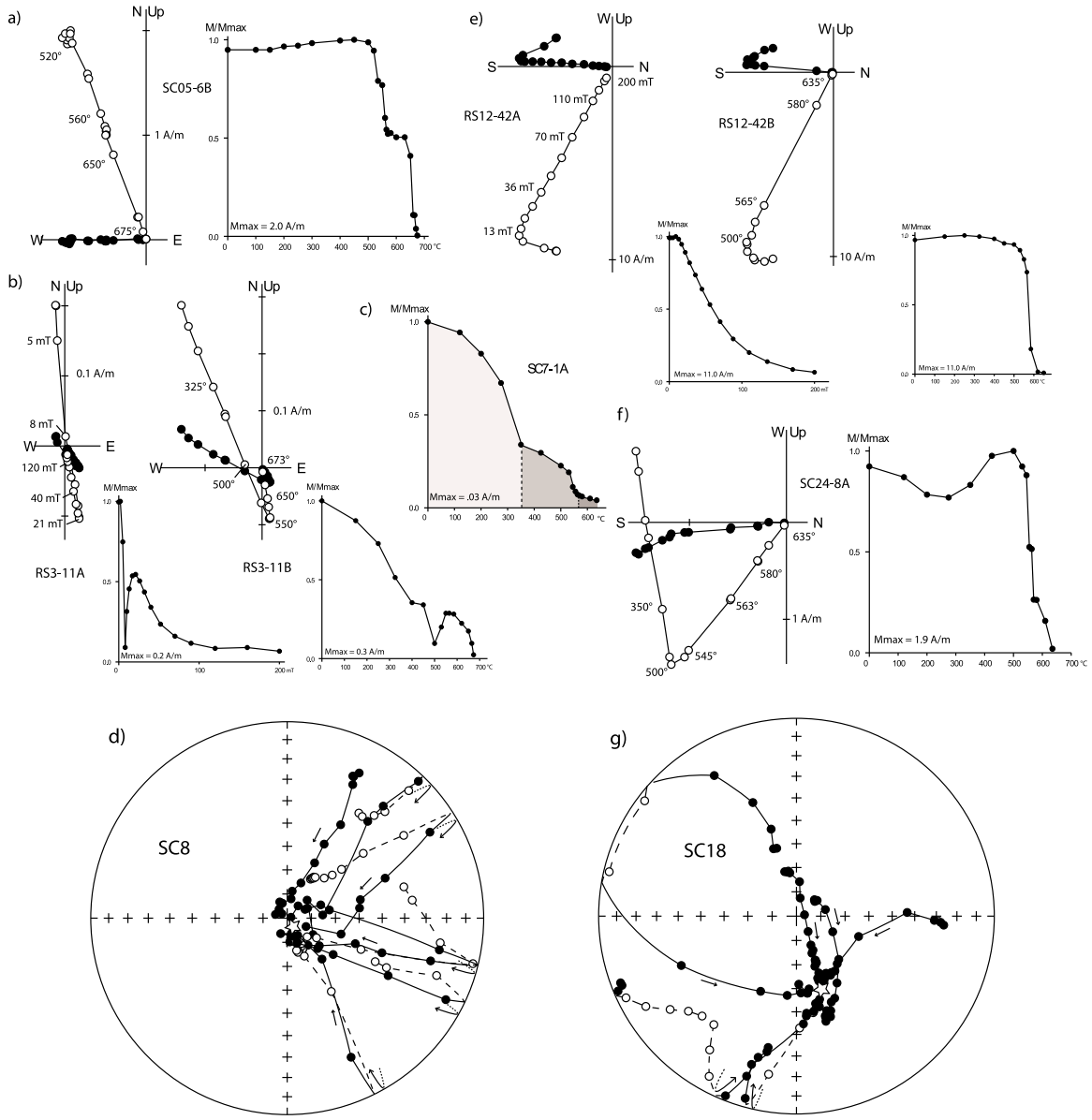

Figure 3. Examples of typical demagnetization behavior. All results are presented in geographic coordinates. In the orthogonal vector diagrams the solid (open) symbols are projections onto the horizontal (vertical) plane. For the stereonets, the solid (open) symbols are projections onto the lower (upper) hemisphere. (a) Locality E, univectorial decay of a component held by two phases with distinct unblocking temperatures. (b) Locality D, two components of magnetization are recognized in both AF and thermal demagnetization diagrams. (c) Locality D, the presence of three phases is suggested by thermal demagnetization spectra; the two lower-temperature phases preserve a parallel direction. (d) Locality D, converging remagnetization circles demonstrate that the less stable components are randomly directed at the site level (overprints), and the components of higher stability are consistent in direction (star). All samples were AF demagnetized. (e) Locality C, comparable results from AF and thermal demagnetization, which reveal the presence of two components of magnetization, although there is no strong evidence for the high-coercive phase. (f) Locality C, two magnetization components are evident in the orthogonal vector diagram, and the thermal demagnetization spectrum suggests that the higher-temperature component is carried by more than one phase. (g) Locality C, converging remagnetization circles again demonstrate the presence of a randomly directed overprint superimposed on a stable direction (star). However, samples from this site do not exhibit evidence of the high-coercive phases, suggesting the stable component partly resides in the low-coercive phase. All samples were AF demagnetized.

Table 1. Site Mean Paleomagnetic Directional Data[a]

Sector	Site	N/n/v	Dg	Ig	Ds	Is	k	α95	Sector/VGP Lat	Sector/VGP Long	A_{95}
A									−37.92	294.53	
	RS16	5/5/5	165.2	56.2	165.2	56.2	50.8	10.8	−78.2	25.7	15.6
	SC19	7/6/1	170.3	47	170.3	47	698.2	3	−77.3	71.8	3.9
	RS15	5/5/2	174.5	59.4	174.5	59.4	110.9	8.3	−85.2	354.8	12.5
	RS13	8/8/8	161.2	58.2	161.2	58.2	160.1	4.4	−75.2	15.1	6.5
	SC18	7/6/3	157.4	62.3	157.4	62.3	118.7	6.6	−72	358.9	10.3
	SC17	-	-	-	-	-	-	-	-	-	
B									−37.91	294.55	
	SC25	7/7/5	164.1	62	164.1	62	89.9	6.6	−76.8	355.6	10.2
	RS12	5/5/5	164.6	63	164.6	63	39.1	12.4	−76.8	350.2	19.5
	SC16	6/6/5	178	58.1	178	58.1	876.7	2.3	−88.2	353.7	3.4
C									−37.90	294.55	
	SC24	7/7/4	175.2	62.6	175.2	62.6	505.5	2.8	−82.9	323.7	4.4
	SC13	7/6/3	179.6	55.3	179.6	55.3	770.1	2.6	−88	106.1	3.7
	RS11	5/5/3	169.6	46.9	169.6	46.9	231.6	5.4	−76.9	70	7
	SC15	5/5/4	178	58.6	178	58.6	278	4.7	−87.9	340.6	7
	SC14	7/7/5	169.5	60.2	169.5	60.2	320.5	3.5	−81.3	359.8	5.3
	RS10	6/6/5	166.4	61.8	166.4	61.8	82.7	6.8	−78.5	354.2	10.4
	SC22	7/4/0	164.1	−62.2	164.1	−62.2	-	12.5	−76.7	354.7	-
	SC23	7/7/6	85.9	70.4	146.7	64.8	158.4	4.9	−64.1	353.8	7.8
D									−37.89	294.57	
	SC12	-	-	-	-	-	-	-	-	-	
	RS09	4/4/2	216.9	77	196.5	53.4	561.9	4.5	−76.1	192.9	6.3
	SC11	7/7/0	165.2	85.9	182.1	61.1	-	9.7	−85.4	274.5	-
	RS08	4/4/0	35	82.7	173.8	71	-	12.2	−72	305.9	-
	SC21	7/5/4	61.7	80.7	163.2	68.7	168.3	6.1	−71.6	328.7	10.3
	RS07	5/5/5	80.3	77.6	155.3	65.3	74.7	8.9	−69.7	349	14.4
	RS06	3/3/2	77.1	80	160.8	66.2	85.7	11.6	−72.5	340.8	19
	RS05	5/4/3	87.4	77.4	155.9	63.7	41	15.4	−70.6	354.3	24.4
	SC08	6/6/4	139.3	86.4	179.5	62.4	113.2	6.6	−84.1	298.1	10.3
	SC10	7/7/4	170.7	85.8	182.9	60.9	29.2	11.9	−85.4	266.9	18.1
	RS03	4/4/4	104.6	75.6	156.2	59.3	74.1	10.7	−71.4	10.2	16.1
	SC09	7/7/7	41.1	86.4	179.3	67.8	159.6	4.8	−77	296.5	8
	RS04	4/4/2	17.1	74.6	167	79.6	121.7	9.7	−57.3	302.8	18.5
	SC07	7/5/0	183.2	80.2	184.5	55.2	-	5.4	−85.8	174.3	-
	SC06	8/7/6	134.3	76.5	166.6	54.9	122.2	5.1	−79	33.3	7.2
	RS02	5/5/5	65	77.6	154.6	68.5	38.3	12.5	−67.4	338.3	21.1
	RS01	-	-	-	-	-	-	-	-	-	
E									−37.87	294.54	
	RS17	6/6/6	261.4	−77.7	344.7	−67.2	41.5	6.8	73.8	151.9	11.3
	SC05	8/8/8	277.6	−73.1	337.1	−62	183.6	2.7	71.8	180.1	4.2
	SC20	6/6/6	304.1	−78.9	353.8	−59.6	188.7	4.9	84.6	174.3	7.4
	SC04	10/10/10	313	−68	344	−50	122.9	3	75.1	228.2	3.9
Mean		N = 35	152.9	74.2	169.2	61.4	95.5	2.5	−80.1	349	3.3

[a]N/n/v indicates (N) number of specimens measured/(n) number of specimens used in site mean calculation/(v) number of directions in (n) that are defined by vectors, rather than great circles. Dg/Ig indicates declination/inclination in geographic coordinates. Ds/Is indicates declination/inclination in stratigraphic coordinates (i.e., tilt corrected). The k indicates the precision parameter of *Fisher* [1953]. The α_{95} indicates the semiangle of the 95% cone of confidence about the site mean direction. VGP lat/long indicates virtual geomagnetic pole latitude/longitude. A_{95} indicates the semiangle of the 95% cone of confidence about the virtual geomagnetic pole.

principal carrier of the B component, which we have assigned the ChRM (Table 1).

[13] Due to limited exposure, the contact between the upper and middle units is poorly defined, but locality C was selected so as to be proximal to the interpolated contact. Demagnetization behavior of rocks from this locality is comparable to that observed in locality D, in that most sites exhibit a minor, randomly directed, low-coercivity/temperature component (A) that is removed prior to a component of higher stability (B) that possesses a magnetization with a consistent direction (Figure 3g). As before, the randomly directed A component is assumed to be a secondary magnetization. AF demagnetization is more successful at component separation,

but thermal demagnetization also shows comparable results (Figure 3e). Thermal demagnetization reveals that the A component is completely unblocked by 585°C, whereas the B component is largely unblocked above 600°C (Figure 3f). As before, these components are interpreted to be typically carried by titanomagnetite and hematite, respectively. In some sites, a high-coercivity phase is not explicitly present, but great circle demagnetization trajectories still track toward a common direction resembling component B, which may be held by a subpopulation of the low-coercivity fraction with a relatively high coercivity (Figures 3e and 3g). Similarly, in some sites that possess both phases, a fraction of the lower-coercivity phase carries a magnetization parallel to the high-coercivity phase (component B), suggesting that remagnetization did not entirely overprint the low-coercivity phase in these sites (Figure 3f). Most of the ChRMs from this locality are south directed with inclinations of about +60° (Table 1). The one exception, SC23, the lowest site at the locality, has a ChRM direction oriented steeply down, parallel to those observed in the D locality of the middle unit. Correspondingly, this site has a structural orientation identical to those exposed at the D locality, suggesting that SC23 is part of the middle unit. SC22, which directly overlies SC23, yields a mean direction parallel to the rest of the sites from the C locality, thus the contact between the middle and upper units may lie between sites SC23 and SC22.

[14] Other sites from the upper section, taken from localities A and B, have demagnetization behavior similar to that observed in locality C. Site SC17, from locality A, has been discarded because all specimens yielded statistically random yet univectorial magnetizations, indicating that it has been completely remagnetized. Consistently high NRM intensities from this site are compatible with the interpretation of lightning-induced contamination. All remaining ChRMs from sites at these localities are south directed with inclinations of about +60°, parallel to the magnetizations observed in locality C (excepting site SC23) (Table 1).

[15] Our overall rejection rate for sites is 8% (3 of 38) and 5% for specimens (11 of 214) (Table 1). Of the retained specimen directions, 70 percent are defined by vectors and 30 percent by great circles. The 35 retained site means were subjected to the bootstrap foldtest, in which tilt corrections are applied to randomly sampled subsets of the original data and directional coaxiality is measured as a function of unfolding [*Tauxe and Watson*, 1994]. After 2000 iterations, the mean degree of unfolding that maximizes directional clustering can be calculated from the collected subset determinations, along with 95% confidence bounds. Field observations show that the upper unit is essentially horizontal, while the middle and lower units may be restored to the paleohorizontal by tilting ~25° around horizontal axes trending 095 and 105, respectively. This 10° distinction in strike does not appreciably affect the outcome of the foldtest. The optimal degree of untilting is 121.5 percent, with 95% confidence limits extending from 105 to 138% (Figures 4a and 4b). This result suggests that if the site mean directions from rocks in the upper and middle/lower sections are from the same population and are reasonably well determined, the magnetization is pretilting, but that the structural dip may be underestimated by 1–9°. Site means were also subjected to the bootstrap reversal test, which evaluates the antipodality of the mean direction of the normal and reverse populations [*Tauxe et al.*, 1991]. Prior to tilt correction, the mean normal direction and inverted mean reverse direction are statistically distinct, but after unfolding the null hypothesis of a common mean cannot be rejected. The tilt corrected population of site-level virtual geomagnetic poles (VGPs) cannot be distinguished from a Fisher distribution at the 95% confidence level (Figure 4c).

[16] The mean direction from the upper unit of this study is statistically different from the mean direction of the upper unit from *Tomezzoli et al.* [2008] (see their Table 1). The directions are distinct in both declination and inclination and, being from the upper unit, are uncomplicated by tilt corrections. The in situ mean directions from the middle units sampled in the two studies are more similar, but the previous collection includes only two sites from the middle section, so a rigorous statistical test of a common mean cannot be applied. Because the populations of data from these two studies do not statistically share a common mean, the data sets have not been combined. The resulting site and unit-level VGPs are listed in Table 1. The study-wide Sierra Chica paleopole, after tilt correction, is: 80.1°S, 349.0°E, A_{95}: 3.3°, K: 53.4, and N: 35. If tilt corrections are optimized by increasing the dip by 5°, the alternative paleopole (SC_{alt}) is: 82.4°S, 6.4°E, A_{95}: 3.0°, K: 68.2.

5. Magnetic Mineralogy

[17] Hysteresis measurements of representative samples throughout the stratigraphic section substantiate the presence of at least two magnetic

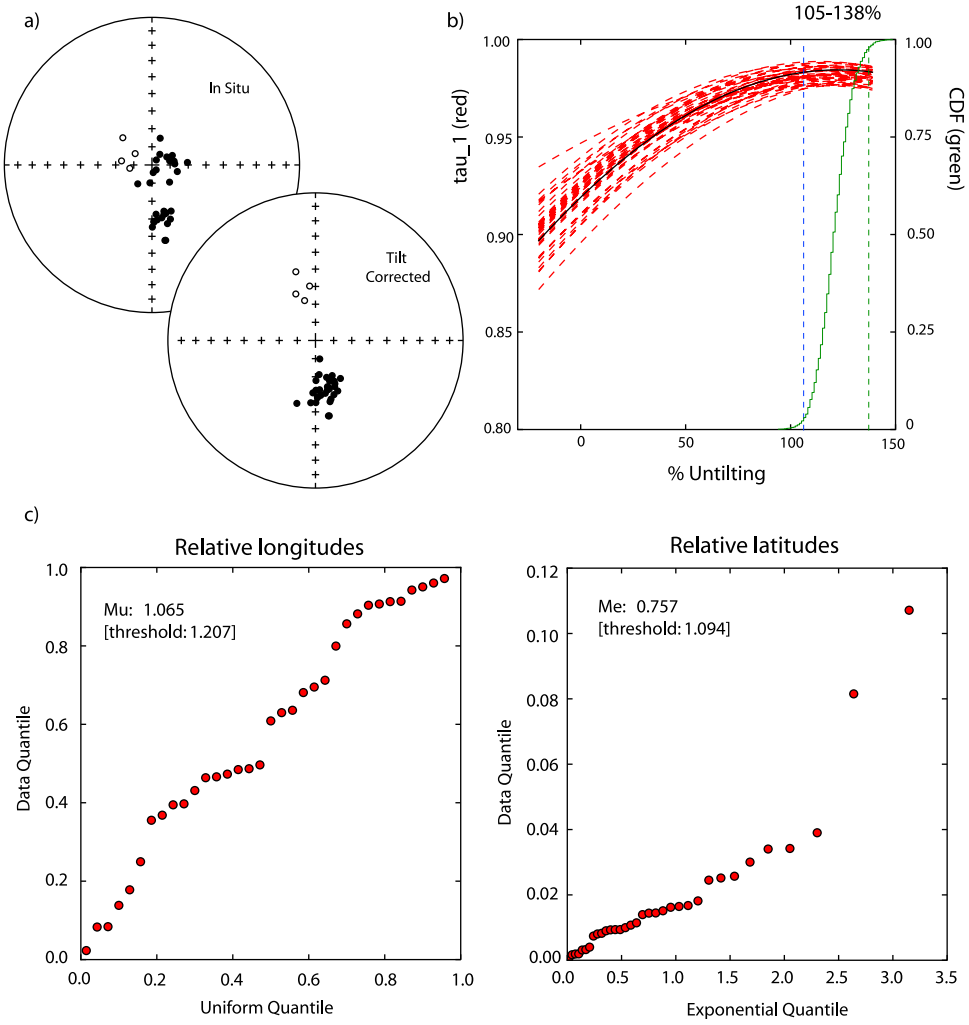

Figure 4. Tilt corrections applied to in situ site mean directions. (a) Mean directions before and after tilt correction. The α_{95} of the means are removed for clarity. (b) Results of the bootstrap fold test. Red dashed lines are example bootstrap results, showing the change in directional clustering (higher tau_1 values = tighter clustering) as a function of unfolding. Cumulative distribution function (green curve) of 2000 bootstrap results shows 95% confidence bounds that extend from 105 to 138% untilting; the optimal value is 121.5%. (c) Quantile-Quantile plots of tilt-corrected site-level virtual geomagnetic poles (VGPs) [*Lewis and Fisher*, 1982]. The plots graphically illustrate the fit of a data set to a theoretical distribution (in this case a Fisher distribution) by the linearity of the data; a perfect fit would result in perfect linearity. Figure 4c (left) compares VGP longitudes (relative to the mean VGP) against a uniform distribution; Figure 4c (right) compares VGP latitudes (relative to the mean VGP) against an exponential distribution, according to *Fisher* [1953]. The values of Mu and Me do not exceed the theoretical thresholds (in brackets) that would permit rejection of the hypothesis that the VGPs are Fisher distributed at the 95% confidence level [see *Tauxe*, 2010].

mineral phases with distinct coercivities (Figure 5), as suggested by AF demagnetizations. Two samples from the upper unit, one from a site with only the low-coercivity phase (SC18-3) and one with both low- and high-coercivity components (SC14-7), were selected for low-temperature remanence and high-temperature susceptibility experiments to further characterize the magnetic carriers. In the FC/ZFC low-temperature experiments, both SC14-7 and SC18-3 experienced a change in the rate of remanence loss during warming through the interval 110–120 K, which is diagnostic of the Verwey transition in magnetite (Figures 6a and 6b) [*Muxworthy and McClelland*, 2000]. In sample SC18-3, this transition appears protracted, perhaps even bimodal, initiating at ~100 K. Such a lowered transition temperature can be a consequence of magnetite nonstoichiometry, either due to impurities or an oxygen deficiency [*Özdemir et al.*, 1993; *Brabers et al.*, 1998]. The suppressed appearance of the transition in sample SC14-7, as well as the gradual remanence loss with warming exhibited

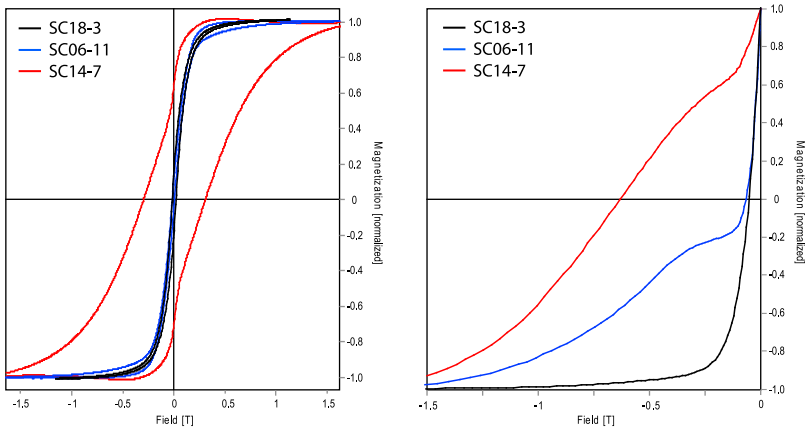

Figure 5. (left) Hysteresis loops after paramagnetic correction and (right) back-field curves of representative samples that exhibit one magnetic phase with a low coercivity (black curves), two magnetic phases with low and high coercivities (blue curves), and dominance by a phase with a high coercivity, but a minor contribution from a phase with a low coercivity (red curves).

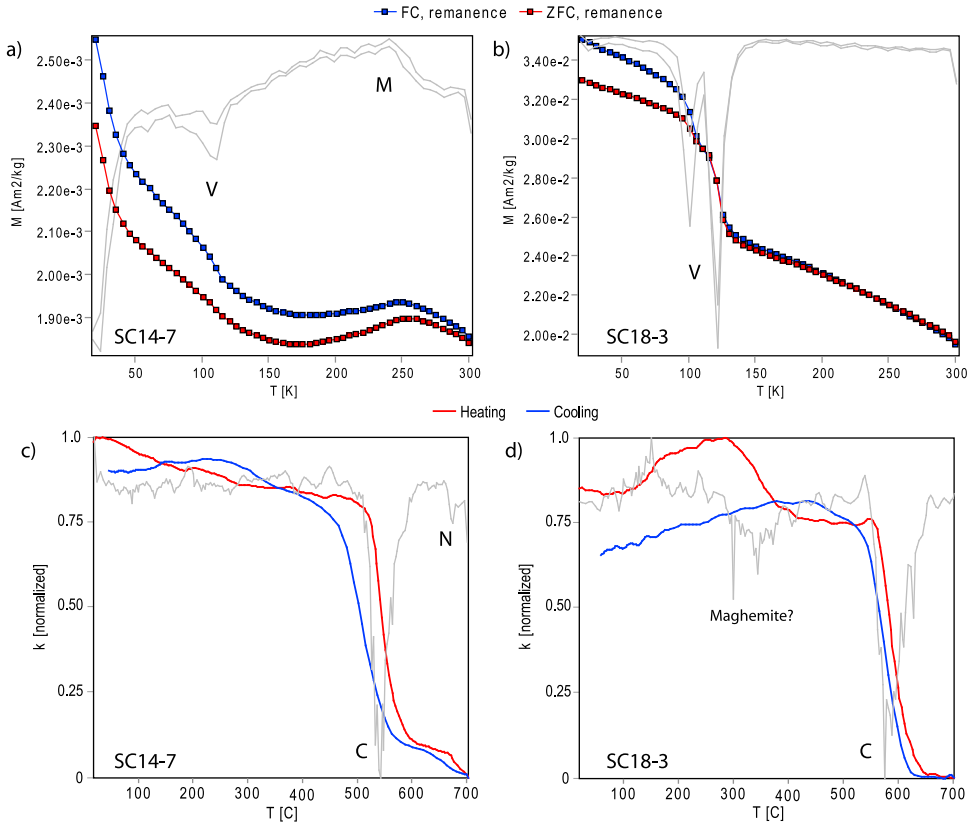

Figure 6. (a and b) Results of low-temperature (remanence) and (c and d) high-temperature (susceptibility) cycling experiments. In Figures 6a and 6b the light gray curves are the first derivatives of the remanence curves. V (Verwey) and M (Morin) denote interpreted transitions discussed in the text. In Figures 6c and 6d the light gray curves are the first derivatives of the heating curve. C and N denote the interpreted Curie and Néel points discussed in the text. Figures 6a and 6c are measurements on a sample possessing both low and high coercivity phases (as determined from demagnetization results), while Figures 6b and 6d are measurements on a sample with only the low coercivity phase.

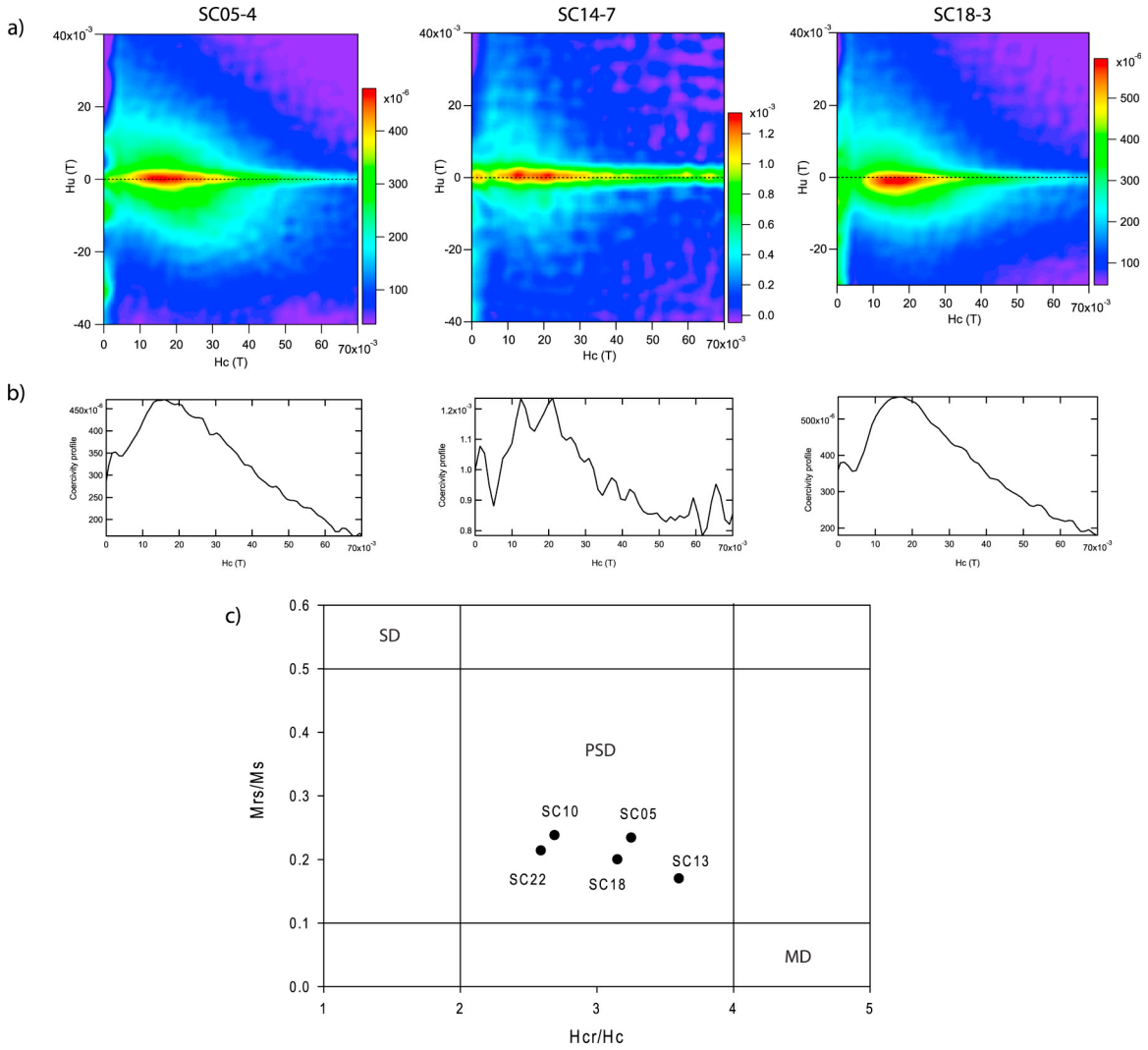

Figure 7. Further documentation of the low-coercivity phase (magnetite). (a) First order reversal curve (FORC) diagrams, showing typical PSD behavior. A smoothing factor of 3 was used in the production of the FORC diagrams. (b) Coercivity profiles taken across the axis Hu = 0. Again, all three samples exhibit very similar PSD behavior. (c) "Day" plot of bulk hysteresis properties of samples dominated by magnetite. All samples fall in the PSD range.

by both samples, could also be indicative of Ti substitution and/or oxidation of magnetite [*Özdemir et al.*, 1993; *Moskowitz et al.*, 1998]. While the remanence of SC18-3 continues to decay monotonically from 120 to 300K, SC14-7 exhibits a broad peak, centered at ~250–260 K, which we interpret to be the expression of the Morin transition in hematite [*Özdemir et al.*, 2008].

[18] Subsamples of SC14-7 and SC18-3 (not used in MPMS experiments) were subjected to thermomagnetic (κ versus T) cycling to identify high-temperature magnetic critical points (Figures 6c and 6d). In SC14-7, inflection points are found at 550°C and 680°C, which are consistent with the Curie temperature of Ti-poor titanomagnetite and the Néel temperature of hematite [*Dunlop and Özdemir*, 1997]. Sample SC18-3 also exhibits a pair of inflection points; at 345°C and 575°C, the latter likely being the Curie point of low-Ti titanomagnetite. The lower temperature critical point is not represented in the cooling curve, implying that it represents a metastable mineralogic phase destroyed during the heating cycle. We interpret this to be the expression of a thermally driven inversion of maghemite to hematite. Maghemite is known to form on the surfaces of magnetite either during primary (deuteric) or secondary low-temperature oxidation [*Dunlop and Özdemir*, 1997]. The low-

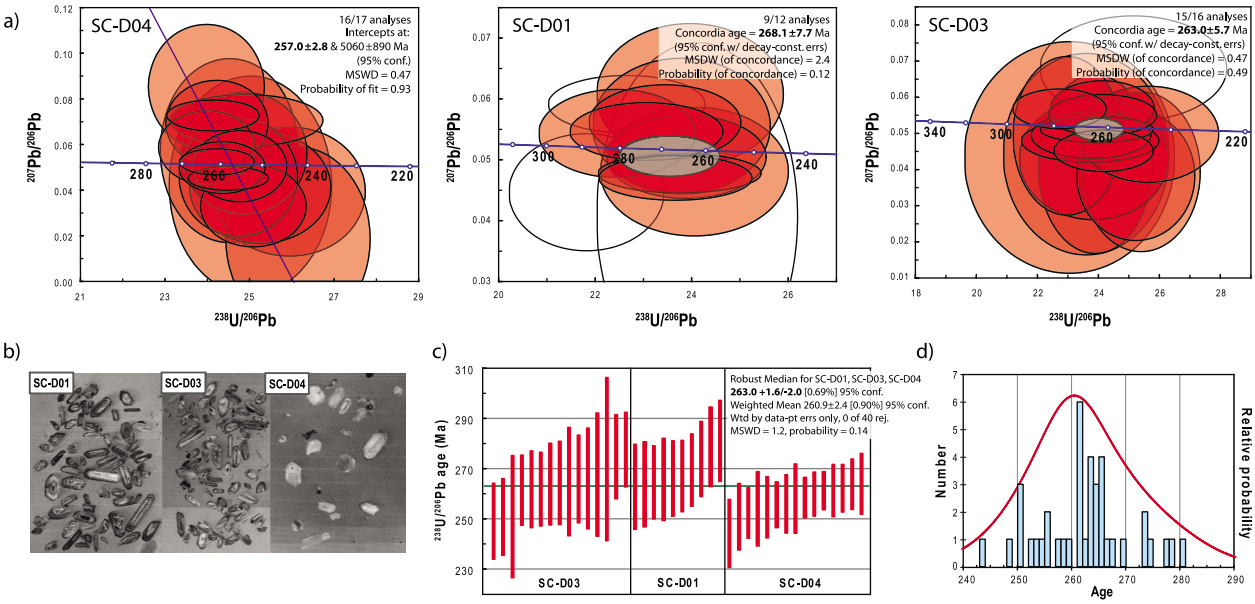

Figure 8. U-Pb SHRIMP geochronology results. (a) Tera-Wasserberg plots of sample results. Unfilled ellipses were not used in the date calculation. All data point error ellipses are 2σ. (b) Cathodoluminescent images of zircon grains used in SHRIMP analysis. (c) Plot of all retained zircon dates with 2σ error (red lines), yielding a robust median age estimate of 263.0 Ma (thick black line). (d) Histogram of all zircon dates showing the mean age estimate of 260.9 Ma.

ered total susceptibility exhibited by the cooling curve is consistent with such a transformation.

[19] FORC diagrams from samples SC14-7 and SC18-3, and sample SC05-4 from the lower unit all exhibit a pattern indicative of pseudo single domain (PSD) sized magnetite: self-closing inner contours and outer contours which diverge toward Hc = 0, with a general asymmetry about the axis Hu = 0 (Figure 7a) [*Roberts et al.*, 2000; *Carvallo et al.*, 2006]. A profile along the axis Hu = 0 demonstrates that the coercivity distribution is very similar between these samples, perhaps reflecting a broad constancy of PSD grain dominance in the magnetite population, as implied by bulk hysteresis data for magnetite dominated samples (Figures 7b and 7c).

6. Geochronology

[20] Three samples were collected for analysis by U-Pb SHRIMP geochronology; SC-D04 (lowest unit), SC-D03 (middle unit), and SC-D01 (upper unit) (Figure 8 and Table 2). Zircon was least abundant in the sample from the lowest trachyandesitic unit, and individual grains showed a greater size variation, ranging from 150 to 500 um. Zircons from SC-D04 also have a more homogeneous internal structure exhibited by the cathodoluminescent images, with grains displaying a more uniformly bright pattern (Figure 8b). Zircons in the samples from the middle and upper rhyolitic units are more abundant and show a homogeneous grain size distribution (about 300 um). These differences between the trachyandesite sample and the rhyolite samples are mirrored by differences in zircon chemistry; the rhyolitic samples are richer in U (average of 150–180 ppm) and have lower average Th/U ratios of about 1.6 (Table 2). Zircon grains from sample SC-D04 present lower average U contents of 70 ppm, and somewhat elevated Th/U ratios >2. Overall, zircon morphologies (euhedral), internal structure (oscillatory zoning, absence of overgrowths) and chemistry (relatively high Th/U ratios) are diagnostic of an igneous origin.

[21] The zircon age populations are relatively homogeneous within each of the samples, and very similar between them (Figures 8a and 8c). Only one zircon xenocryst was observed, in sample SC-D03 (which provides a U-Pb date of 690 ± 18 Ma; 2σ error); it was likely inherited from underlying Precambrian basement during magma ascent and emplacement. Zircons from SC-D03 display the most uniform distribution of age estimates, with 15 of the 16 grains yielding a U-Pb "concordia" date of 263.0 ± 5.7 Ma with a low MSWD of 0.47. A slightly older date of 268.1 ± 7.7 Ma is calculated for sample SC-D01, with a higher MSWD of 2.4. These age estimates are equivalent at the 2σ

Table 2 (Sample). SHRIMP U-Pb Geochronology Data[a] [The full Table [2] is available in the HTML version of this article]

Sample Name and Spot	% $^{206}Pb_c$	ppm U	ppm Th	$^{232}Th/^{238}U$	ppm $^{206}Pb^*$	$^{206}Pb/^{238}U$ Age[b]	$^{206}Pb/^{238}U$ Age[c]	$^{206}Pb/^{238}U$ Age[d]	$^{207}Pb/^{206}Pb$ Age[b]
Sierra Chica SC-D01									
SC-D01-12	0.94	102	137	1.38	3.69	262.5 ± 8.5	263.6 ± 8.6	264 ± 11	105 ± 210
SC-D01-3	-	163	191	1.21	5.78	263.5 ± 8.5	260.5 ± 8.4	259 ± 10	630 ± 170
SC-D01-8	0.47	141	192	1.40	5.11	264.3 ± 7.3	264.6 ± 7.4	265 ± 9.6	220 ± 130
SC-D01-11	1.50	81	105	1.33	2.97	265.5 ± 8.2	264.2 ± 8.2	264 ± 11	434 ± 180
SC-D01-4	0.39	309	561	1.87	11.2	265.9 ± 7.6	267.1 ± 7.7	267 ± 11	90 ± 65
SC-D01-10	0.59	269	466	1.79	9.83	266.8 ± 7.1	268.3 ± 7.3	269 ± 10	52 ± 76
SC-D01-7	-	265	411	1.60	9.67	269.3 ± 7.2	267.8 ± 7.2	268.1 ± 9.8	460 ± 99
SC-D01-2	-	177	273	1.59	6.59	273.6 ± 7.5	272.6 ± 7.6	275 ± 10	399 ± 80
SC-D01-9	-	146	324	2.29	5.58	280.9 ± 8.1	280.1 ± 8.1	277 ± 13	386 ± 120
SC-D01-6[e]	-	149	141	0.98	5.62	278.5 ± 8	276 ± 8	276.6 ± 9.4	570 ± 71
SC-D01-5[e]	2.72	39	41	1.09	1.44	261.9 ± 9	265.4 ± 8.7	273 ± 11	−311 ± 740
SC-D01-1[e]	0.73	97	103	1.10	3.83	288.7 ± 8.4	291.4 ± 8.6	292 ± 10	−75 ± 210
Average	0.38	161.66	245.35	1.47					
SD	1.06	82.16	163.18	0.38					
Sierra Chica SC-D03									
SC-D03-3	1.66	100	100	1.04	3.4	246.5 ± 8.8	246.9 ± 8.8	245 ± 11	181 ± 260
SC-D03-2	1.96	60	88	1.50	2.08	248.8 ± 7.6	252.5 ± 7.3	254.6 ± 9.8	−398 ± 600
SC-D03-4	2.04	47	54	1.17	1.65	250.5 ± 7.7	254.6 ± 7.7	256.9 ± 9.5	−476 ± 510
SC-D03-17	0.93	269	436	1.68	9.63	261.2 ± 7	263.3 ± 7.1	263.3 ± 9.8	−49 ± 130
SC-D03-12	-	95	138	1.49	3.39	261.6 ± 7.7	260.4 ± 7.7	259 ± 10	414 ± 94
SC-D03-6	-	139	213	1.59	4.9	261.6 ± 7.4	259.8 ± 7.3	261.1 ± 9.9	493 ± 120
SC-D03-5	0.04	332	558	1.74	11.9	263.6 ± 8.2	263.8 ± 8.2	262 ± 12	242 ± 66
SC-D03-8	1.88	97	165	1.76	3.54	264.1 ± 8.3	267.4 ± 7.9	261 ± 11	−266 ± 620
SC-D03-9	1.47	116	176	1.56	4.25	265 ± 11	267 ± 11	267 ± 15	−177 ± 400
SC-D03-13	0.24	338	470	1.44	12.3	265.7 ± 8.7	266.4 ± 8.8	265 ± 12	168 ± 130
SC-D03-14	0.56	192	223	1.20	7	266 ± 10	267 ± 10	266 ± 13	93 ± 120
SC-D03-16	2.57	62	121	2.00	2.33	267 ± 12	270 ± 12	277 ± 18	−102 ± 640
SC-D03-11	5.62	92	178	1.99	3.64	274 ± 16	276 ± 16	277 ± 25	−153 ± 750
SC-D03-15	1.32	78	144	1.91	2.95	274.5 ± 8.4	275.4 ± 8.1	275 ± 12	160 ± 430
SC-D03-10	-	301	744	2.55	11.3	277.4 ± 7.5	275.7 ± 7.5	273 ± 13	482 ± 88
SC-D03-1[e]	-	55	67	1.26	1.85	251 ± 12	246 ± 12	244 ± 15	830 ± 190
SC-D03-7[e]	0.03	753	339	0.47	73.1	690 ± 18	691 ± 18	690 ± 19	648 ± 18
Average	1.07	183.99	247.83	1.55					
SD	1.58	177.64	195.44	0.46					
Sierra Chica SC-D04									
SC-D04-2	2.92	37	71	2.00	1.29	250.6 ± 6.7	253.7 ± 6.2	258.4 ± 10.2	−282 ± 619
SC-D04-3	2.44	31	47	1.55	1.11	254.3 ± 6.1	252.8 ± 5.4	254.5 ± 8.1	460 ± 430
SC-D04-4	0.93	126	170	1.39	4.47	258.2 ± 4.0	260.2 ± 4.1	260.3 ± 5.5	−53 ± 113
SC-D04-5	1.08	83	102	1.26	2.92	255.4 ± 4.6	255.7 ± 4.3	257.5 ± 5.7	212 ± 292
SC-D04-6	0.84	128	167	1.35	4.56	259.7 ± 4.4	260.2 ± 4.2	263.4 ± 5.6	185 ± 218
SC-D04-8	1.71	43	116	2.77	1.54	255.7 ± 5.8	257.5 ± 5.1	249.5 ± 11.0	−24 ± 562
SC-D04-10	2.30	65	182	2.87	2.22	243.9 ± 6.8	247.4 ± 6.1	242.3 ± 12.8	−401 ± 768
SC-D04-11	3.04	48	141	3.00	1.71	252.1 ± 5.1	257.8 ± 4.9	265.0 ± 11.3	−883 ± 641
SC-D04-12	−3.01	49	56	1.17	1.71	263.7 ± 6.1	252.8 ± 4.8	255.9 ± 6.3	1319 ± 255
SC-D04-13	1.34	56	157	2.91	1.99	257.9 ± 6.9	256.0 ± 4.7	260.6 ± 10.5	500 ± 634
SC-D04-14	−0.20	52	145	2.86	1.86	262.0 ± 4.8	255.2 ± 4.8	255.9 ± 10.6	1002 ± 78
SC-D04-15	3.18	56	86	1.59	2.07	263.5 ± 5.1	261.3 ± 4.8	263.1 ± 7.3	550 ± 246
SC-D04-17	0.64	277	1075	4.01	9.91	261.0 ± 3.8	260.7 ± 3.8	268.6 ± 11.6	300 ± 102
SC-D04-18	−1.46	55	109	2.05	1.92	261.0 ± 5.3	255.3 ± 4.7	254.1 ± 7.8	904 ± 229
SC-D04-19	−1.01	29	51	1.80	0.998	253.7 ± 7.4	247.7 ± 7.3	254.0 ± 11.1	941 ± 135
SC-D04-16[e]	6.61	29	63	2.26	1.06	252.8 ± 7.9	255.7 ± 5.6	250.1 ± 11.0	−221 ± 1166
SC-D04-7[e]	6.19	52	134	2.66	1.83	242.1 ± 6.4	251.8 ± 4.7	248.6 ± 9.8	−2636 ± 3609
SC-D04-20[e]	1.86	28	38	1.41	1.05	273.3 ± 7.6	270.5 ± 6.2	274.3 ± 8.9	601 ± 517
Average	1.63	69.22	161.65	2.16					
SD	2.39	59.56	232.67	0.80					

[a]Errors are 1σ. Pb_c and Pb* indicate the common and radiogenic parts, respectively. Error in standard calibration was 0.92% (not included in listed errors but required when comparing data from different mounts).
[b]Common Pb corrected using measured ^{204}Pb.
[c]Common Pb corrected by assuming $^{206}Pb/^{238}U$-$^{207}Pb/^{235}U$ age concordance.
[d]Common Pb corrected by assuming $^{206}Pb/^{238}U$-$^{208}Pb/^{232}Th$ age concordance.
[e]Analysis not used in final date calculation.

error level. SC-D04 yields the youngest date of 257.0 ± 2.8 Ma, calculated from a line intercepting the concordia curve in the Tera-Wasserberg plot. This age estimate is significantly younger than those calculated from the samples from overlying units. However, the lower U abundances in this sample signify a higher proportion of common Pb, as indicated by the presence of ^{204}Pb. We regard the data from the two rhyolitic samples as the most robust.

[22] For paleomagnetic purposes, these three units are interpreted to represent closely spaced magmatic episodes that reflect emplacement over a million year timescale, which should be sufficiently long to average effects of secular variation, but certainly not long enough to record appreciable plate motion. We therefore treat these samples as a single magmatic episode and pool the geochronologic data from the three samples. The median date calculated from the three samples (263.0 +1.6/−2.0 Ma, 0.69%, 95% conf) is statistically indistinguishable from the well-determined age estimate of sample SC-D03.

7. Discussion

7.1. Interpretation of Paleomagnetic Results

[23] The presence of normal polarity magnetizations in the lower unit suggests that the Sierra Chica is younger than the Kiaman Reversed Superchron, which has an upper age of about 265 Ma [*Gradstein et al.*, 2004]. This is compatible with our new U-Pb age estimate of 263.0 +1.6/−2.0 Ma for the Sierra Chica. However, if the rocks were not magnetized during a protracted interval of reverse polarity, the dominance of reverse polarity magnetizations in the middle and upper units suggests that it may not adequately average secular variation. The upper unit is notable in this regard; the 15 site-level VGPs are very well clustered with an A_{95} of 3.5° and a K of 122. Using the mean value of K (at latitude ≈ 42°) determined from a compilation of volcanic rock paleomagnetic records from the last 5 Myr [*Harrison*, 2009], and the secular variation averaging χ^2 test of *McFadden* [1980], a VGP set of N = 15 is expected to yield a K of 20.3 to 49.6 (95% confidence limits), if secular variation has been adequately averaged. The tight clustering of the upper unit VGPs can be attributed to rapid flow emplacement, and may suggest that the upper unit represents one large eruptive event. This is further supported by the thick and featureless character of the upper unit, and the scarcity of identified cooling contacts within it. The lower and middle units, with thinner flows with abrupt changes in characteristics and distinct cooling contacts, are more likely to represent a prolonged series of eruptions. This is reflected in a higher A_{95} (5.2° after tilt correction), a smaller K (40.7) and dual polarity magnetizations. The expected range for K (determined as above with N = 20) is 21.3 to 45.7 (95% confidence limits).

[24] If the upper unit was largely emplaced during one eruptive event, it is plausible that the tilting of the middle/lower units could have been a consequence of local subsidence or caldera collapse, due to the rapid evacuation of large quantities of magma. In a multicyclic eruptive center, it is likely that early eruptive phases become structurally modified by later eruptive events [*Lipman*, 1997]. An alternative interpretation involving tilting driven by regional deformation seems less likely, given the short time span between emplacement of the lower/middle and upper units, based on the U-Pb dates.

[25] It was previously noted that the optimal degree of unfolding is greater than 100 percent and possibly indicates an underestimate of the true tectonic tilt of the lower/middle units. It is important to note that original horizontality cannot always be assumed with silicic volcanic rocks, due to their relatively high viscosity. Although we are unable to unequivocally eliminate this possibility, we recognize that the character (thinner, lithic rich) of the dipping lower/middle units is indicative of volatile-charged (fluidized) flow, which is unlikely to assume steep gradients during emplacement. An ongoing magnetic fabrics study may be able to confirm this assumption in the future.

[26] The bootstrap foldtest seeks to maximize the coaxiality of a population of directions, but this expectation is only exactly appropriate if two populations of directions are of the same age (and technically error free). Our U-Pb dates indicate that the lower, middle, and upper units are approximately the same age, having been emplaced over a million year timescale. Thus, the condition of age equivalence seems to be met; however, the results of the secular variation averaging χ^2 test suggest that the upper unit was magnetized over a relatively brief interval of time, and so its population of magnetization directions may more closely represent an instantaneous paleomagnetic field rather than a time-averaged one. In this case, maximizing the coaxiality of the population of directions from the lower/middle and upper units is unlikely to be exactly appropriate, as the lower/middle units have collectively averaged secular variation, while the upper unit has not.

Therefore, we do not necessarily consider the optimal foldtest result (SC_{alt}) to be the most reliable estimate of the true paleomagnetic pole.

[27] The positive reversal test based on the complete data set supports our contention that the collection as a whole reflects a sufficiently time-averaged sampling of the paleomagnetic field, and that the populations are directionally similar. The recognition of PSD magnetite and hematite as the carriers of the ChRM, which are capable of acting as high-fidelity magnetic recorders across geologic timescales, is consistent with the interpretation of a primary magnetization [*Dunlop and Özdemir*, 1997]. Ultimately, the Sierra Chica paleopole meets 6 of the 7 reliability criteria as proposed by *Van der Voo* [1990]; it does not meet criterion #7, as it resembles Late Cretaceous South American paleopoles [*Somoza and Zaffarana*, 2008].

7.2. Implications

[28] Most paleomagnetic poles that constitute the Late Paleozoic–Early Mesozoic APWP of South America are derived either from relatively old studies, which do not meet modern reliability criteria, or sedimentary rocks, which are prone to misrepresenting the paleomagnetic field via effects of inclination shallowing, and are often associated with poor absolute age control. A total of 27 South American paleomagnetic poles with inferred ages of 200 to 300 Ma meet reliability criteria #2 (sufficient number of samples: $N \geq 6$, $n \geq 30$) and #3 (adequate demagnetization) [*Van der Voo*, 1990] (Table 3). Of the 27 compiled poles, seven are derived from postfolding magnetizations with no upper age constraints, and are instead dated by the relative position of the pole with respect to previously published results. The use of such poles in the construction of an APWP or as reference poles involves circular reasoning, and these poles will not be considered further. We discard four additional poles due to poor structural control, in that they are suspected to have been subjected to vertical axis rotations or that the structural restorations are either unknown or complex. Of the remaining 16 poles, three are defined by synfolding magnetizations from sedimentary sequences that were deformed during the SROP. Because the timing of SROP deformation is poorly established, the age constraints on these magnetizations are relatively limited. Only seven of the 16 filtered results include data derived from igneous rocks, and of the nine studies conducted entirely on sedimentary rocks, only two were explicitly checked/corrected for the effects of inclination shallowing. Furthermore, none of the igneous rocks examined have been recently or reliably dated by modern geochronologic methods, the few existing isotopic age estimates having been obtained by the demonstrably inferior K-Ar technique. Thus, our new data provide a well-dated, high-quality paleomagnetic pole for this critically data deficient segment of the South American APWP.

[29] Our new paleopole (SC) is proximal to the Late Permian mean pole calculated from the filtered compilation (Figure 9 and Table 3). Because of the sparsity of poles and the poor chronologic resolution on several sequences, only three mean paleopoles were calculated from the filtered compilation (for the Early Permian, Late Permian, and Triassic), and several results were included in two mean pole calculations, so the estimates are not strictly independent. To allow for a meaningful comparison, SC was not included in the calculation of the Late Permian mean pole (Figure 9). We note that SC is observed to fall within the A_{95} of this Late Permian mean pole, whereas SC_{alt}, the pole obtained by alternatively adopting the structural correction that optimizes directional clustering, lies outside this A_{95}. SC is significantly different from the previous pole from the Sierra Chica (pSC), which appears to fall closer to the Early Permian mean pole, but with a notably different longitude (Figure 9).

[30] Despite the overall scatter of poles in this filtered compilation, there is a clear change in pole position as a function of inferred pole age (path A, Figure 10), which is consistent with the combined Late Paleozoic–Early Mesozoic APWPs of other Gondwana blocks rotated into a common reference frame (path B, Figure 10; data from compilation in the study by *Torsvik et al.* [2008]). The trajectory of Path B corroborates the mid-to-Late Permian curvature evident in path A, which SC seems to further support [see also, *Tomezzoli*, 2009]. It is important to note that paths A and B, although similar in trend, are not coincident for the mid-to-Late Permian time period. In the same way, the combined APWPs of Baltica and Laurentia, rotated into the same South American reference frame (path C, Figure 10; data from compilation in the study by *Torsvik et al.* [2008]), show a similar form to path A, but diverge from it most obviously in the mid-to-Late Permian. Yet, the most pronounced disparity in the mid-to-Late Permian is between paths B and C, a discrepancy that has been long recognized and enduring [*Irving*, 2004]. The fact that the filtered South American data set and the SC result "bisect" the separation of the B and C paths

Table 3. Paleopoles of the Inferred Age Range of 300–200 Ma From South America[a]

Pole	Rock Unit	Type	Age	Plat	Plon	$Plat_{co}$	$Plon_{co}$	N	A95	Notes	Reference
1	Dolerites, Suriname	I	~200 Ma[b]	−82	320	−82.5	295.8	10	10		*Veldkamp et al.* [1971]
2	Rio Blanco, Uspallata, Argent.	S, E	lTr	−81.8	298.3	−81.8	298.3	12	7.6		*Vizan et al.* [2004]
3	Rio Curaco, Carapacha Basin, Argent.	S, I	242 ± 10 Ma (K-Ar)	−64	5	−64	5	13	5	1	*Tomezzoli et al.* [2006]
4	Mitu Group, Peru	S, E	lP-eTr	−71.4	303.6	−71.4	293.5	6	5.7		*Gilder et al.* [2003]
5	Pavon Formation, SRB, Argent.	S, I	260–240 Ma (K-Ar)	−83.7	271	−83.7	271	11	7.9	1	*Rapalini and Cingolani* [2004]
6	Cerro Victoria, Rio de la Plata, Argent.	S	lP-eTr	−82.6	309.3	−82.4	303.3	13	3.9	1	*Rapalini and Sánchez Bettucci* [2008]
7	Yerbal, Rio de la Plata, Argent.	S	lP-eTr	−77	298.4	−76.6	294.9	6	5.9	1	*Rapalini and Sánchez Bettucci* [2008]
8	Rocha, Rio de lat Plata, Argent.	S	lP-eTr	−76.6	291	−76.2	287.7	18	4.2	1	*Rapalini and Sánchez Bettucci* [2008]
9	Independencia Group, Paraguay	S	lP (post-Kiaman)	−80.7	7	−83.6	355.8	10	6.6	[c]	*Rapalini et al.* [2006]
10	Quebrada del Pimiento Formation, SRB, Argent.	I	260 Ma (K-Ar)	−65.9	189.8	−65.9	189.8	7	11.8	2	*Terrizano* [2005]
11	La Flecha, Precordillera, Argent.	S	lP? (post-Kiaman)	−63.8	244.6	−63.8	244.6	7	18	1	*Rapalini and Astini* [2005]
12	Tambillos, Uspallata Basin, Argent.	E	late eP-lP (Kiaman)	−78.9	319.6	−78.9	319.6	16	6.5		*Rapalini and Vilas* [1991]
13	Horcajo Formation, Uspallata Basin, Argent.	E	lP (Kiaman)	−72.4	264.8	−72.4	264.8	26	12		*Rapalini and Vilas* [1991]
14	La Colina Formation-Paganzo Village, Argent.	S	266 ± 7 Ma (K-Ar)	−80.6	268.8	−80.6	268.8	162	2.8	2	*Geuna and Escosteguy* [2004]
15	Tunas II, Sierra Australes, Argent.	S	eP-lP (Kiaman)	−74.1	25.9	−74.7	23.6	24	5.2	3	*Tomezzoli* [2001]
16	Choiyoi, Cerro Chachil, Argent.	E	eP-lP (Kiaman)	−21	232	−21	232	n = 33	8	2	*Rapalini et al.* [1989]
17	Multiple Formations, E. Cordillera, Bolivia	S	eP-lP (Kiaman)	−81.8	344.2	−83.7	322.7	57	3.5		*Libarkin et al.* [1998][d]
18	Sierra Grande-San Carlos Mem., Argent.	S	eP-lP (Kiaman)	−77.3	310.7	−77.3	310.7	13	7	3	*Rapalini* [1998]
19	Zonda and San Juan Formations, Argent.	S	P? (Kiaman)	−68.9	346.9	−68.9	346.9	11	17.8	1	*Rapalini and Tarling* [1993]
20	Cerro Colorado, Paganzo Basin, Argent.	S	lCr-lP (Kiaman)	−79.3	290.6	−79.3	290.6	6	11		*Geuna and Escosteguy* [2004]
21	Copacabana Group, Peru	S	eP	−68	321	−69.1	312.7	9	5.2		*Rakotosolofo et al.* [2006]

Table 3. (continued)

Pole	Rock Unit	Type	Age	Plat	Plon	$Plat_{co}$	$Plon_{co}$	N	A95	Notes	Reference
22	Tunas I, Sierra Australes, Argent.	S	eP (Kiaman)	−63	13.9	−63.6	12	19	5.1	3	*Tomezzoli and Vilas* [1999]
23	Pular/Cas Formations, Chile	E	290 ± 7 Ma (K-Ar)	−57	350	−57	350	10	9.6		*Jesinkey et al.* [1987]
24	Rincon Blanco, Argent.	S,E	295–287 Ma (K-Ar)	−75	291.5	−75	291.5	19	6.7	2	*Geuna and Escosteguy* [2004]
25	La Tabla Formation, Chile	E	lCr-eP	−51	347	−51	347	10	5.7		*Jesinkey et al.* [1987]
26	La Colina Formation-Las Mellizas, Argent.	S	295 ± 5 Ma (K-Ar)	−52.4	341.6	−52.4	341.6	63	4.9		*Geuna and Escosteguy* [2004]
27	Santa Fe Goup, Brazil	S	lCr-eP (Kiaman)	−62.5	328.3	−64	322.1	60	4.1	[c]	*Brandt et al.* [2009]
pSC	Sierra Chica, La Pampa, Argent.	E	263 +1.6/−2.0 Ma	−64	17	−64	17	10	15		*Tomezzoli et al.* [2008]
SC	Sierra Chica, La Pampa, Argent.	E	263 +1.6/−2.0 Ma	−80.1	349	−80.1	349	35	3.3		This Study
Sc_{alt}	Sierra Chica, La Pampa, Argent.	E	263 +1.6/−2.0 Ma	−82.4	6.4	−82.4	6.4	35	3		This Study

Mean Poles	Pole Used	Label	Age	$Plat_{co}$	$Plon_{co}$	Np	A95
Triassic	1, 2, 4	Tr	250–200 Ma	−78.6	295.2	3	9.5
Late Perm.	4, 9, 12, 13, 15, 17, 18	lP	275–250 Ma	−80.1	314.2	7	7.3
	Late Permian mean pole with SC			−80.3	318.4	8	6.4
Early Perm.	15, 17, 18, 20–23, 25–27	eP	300–275 Ma	−68.9	340.4	10	8.9

[a]Type indicates rock type; S indicates sedimentary; I indicates intrusive; E indicates extrusive. Age indicates best estimate of age of magnetization. Plat/Plon indicate paleopole latitude/longitude. $Plat_{co}$/$Plon_{co}$ indicate paleopole latitude/longitude after rotation into Colorado (central Argentina) Plate reference according to *Torsvik et al.* [2009]. N(n) indicates number of sites(samples). A_{95} indicates the semiangle of the 95% cone of confidence about the virtual geomagnetic pole. Notes: 1 indicates no robust age constraints, age estimated from APWP placement; 2 indicates poor structural control; 3 indicates syntectonic magnetizations (timing of magnetization is loosely constrained).
[b]Estimate from *Nomade et al.* [2007].
[c]Checked/corrected for inclination shallowing.
[d]Reinterpreted by *Gilder et al.* [2003].

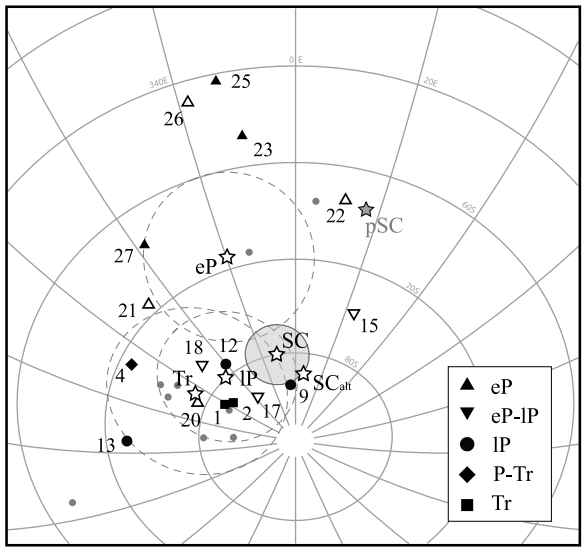

Figure 9. Paleopoles of the inferred age range of 300–200 Ma from South America. Numbers correspond to pole numbers in Table 3. Symbol shapes correspond to age as follows: upright triangles indicate Early Permian, inverted triangles indicate mid-Permian, circles indicate Late Permian, diamonds indicate Permo-Triassic, and squares indicate Triassic. Solid symbols are poles that are at least partly derived from igneous rocks or are results from sedimentary rocks that have been checked/corrected for inclination shallowing; open symbols are therefore considered to be "less-reliable" results. Small gray dots are the poles listed in Table 3 that were rejected according to notes 1 or 2. SC indicates Sierra Chica result (this work), and SC_{alt} indicates Sierra Chica result with optimal untilting. The pSC indicates Sierra Chica result of *Tomezzoli et al.* [2008]. Open stars correspond to mean poles in Table 3: eP indicates Early Permian, lP indicates Late Permian, and Tr indicates Triassic. A_{95} from all but SC and the mean poles have been removed for clarity.

would suggest that the disparity is in part a consequence of inclusion of poor-quality results, rather than a reconstruction problem or a geomagnetic field aberration. Indeed, within the South American data set, the poles that fall the closest to the Permian segment of path B are those derived from sedimentary rocks (and uncorrected for inclination shallowing). Similarly, Late Paleozoic–Early Mesozoic South American paleopoles rejected on the basis of failing to meet reliability criterion #2 or #3 (and therefore not shown) are generally closer to path B than high-quality age-equivalent poles. This may suggest that path B (and perhaps path C) may be contaminated by systemic data pathologies, such as unrecognized or incompletely removed overprints, inclination shallowing, structural complexities, or erroneous age assignments. Although an in-depth analysis of these larger pole sets is outside of the scope of this paper, we note that early paleomagnetic results and those derived from sedimentary sequences constitute a significant part of the collections, as seen in the South American data set. Although errors in Euler rotations undoubtedly remain and contribute to these APWP discrepancies, we posit that paleomagnetic data of relatively poor quality are the principal source of the problem. This hypothesis implies that controversial Late Permian–Early Triassic paleogeographic reconstructions built to accommodate the paleomagnetic data [*Irving*, 1977, 2004; *Torcq et al.*, 1997] are not necessary, but additional work is required to demonstrate this unequivocally. For times before the mid-to-late Early Permian (>~280 Ma), a Pangea "B-type" configuration remains a possibility [*Muttoni et al.*, 1996, 2003].

8. Conclusions

[31] A joint paleomagnetic and geochronologic reexamination of the Sierra Chica has resulted in a

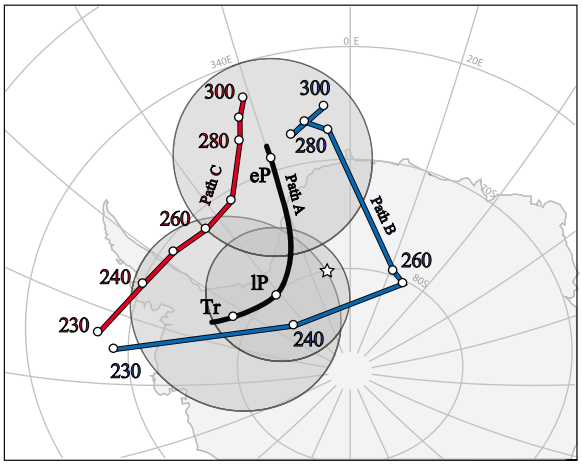

Figure 10. Comparison of apparent polar wander paths in a Pangea A–type reconstruction [see *Torsvik et al.*, 2008]. Path A is defined by three mean poles from Table 3: eP indicates Early Permian, lP indicates Late Permian (with SC result included), and Tr indicates Triassic. The black line connects the poles, assuming a simple path. Path B (combined data from India-Pakistan, Madagascar, and Africa [*Torsvik et al.*, 2008]) and Path C (combined data from Baltica and Laurentia [*Torsvik et al.*, 2008]) have been rotated into the Colorado (central Argentina) Plate reference frame [*Torsvik et al.*, 2009]. Baltica and Laurentia data have been combined via the Euler pole of *Alvey* [2009]. Paths B and C are moving averages, constructed by a moving 20 Myr window, with 10 Myr steps. Ages (Ma) are listed adjacent to select poles. A_{95} from these paths have been removed for clarity. The star is the new SC pole.

new high-quality Late Paleozoic paleomagnetic pole for Gondwana. New U-Pb age determinations indicate that the Sierra Chica was emplaced at 263.0 +1.6/−2.0 Ma. Positive fold and reversal tests demonstrably show the magnetization to be primary, and rock magnetic tests indicate that the carriers of magnetization are PSD magnetite and fine hematite, which are geologically stable and capable of preserving a primary Late Permian remanence. The position of the Sierra Chica pole (80.1°S, 349.0°E, A_{95}: 3.3°) is proximal to the Late Permian mean pole for South America, calculated from a filtered paleopole data set that yielded few, but moderately reliable records. The Sierra Chica pole, therefore, corroborates the position of this Late Permian mean pole, as well as the curvature of the Late Paleozoic segment of the APWP of Gondwana. The relative position of this new high-quality paleomagnetic pole between the previously distinct Late Permian segments of the Laurussian and Gondwanan APWPs suggests that the inferred separation between the paths is due to systemic data pathologies.

Acknowledgments

[32] The authors thank H. Tickyj and M. E. Woroszylo for discussions about the area and assistance in the field. Mike Jackson and the staff at the IRM are thanked for their assistance with the rock magnetic experiments. We also acknowledge the use of the following freeware: Paleomac, PmagPy, Gmap, and FORCinel. Financial support for this research was provided by the Norwegian Geological Survey (NGU) and the U.S. National Science Foundation, Division of Earth Sciences (Tectonics Program) and Office of International Science and Engineering (Americas Program), grant EAR-0634807 and is gratefully acknowledged. Additional funding was provided by PIP-CONICET 11220080102828, UBACYT X220, and an IRM visiting fellowship granted to M. Domeier. E. Tohver acknowledges funding from the Australian Research Council (LP0991834) and use of the UWA-Curtin joint facilities for imaging (Centre for Microscopy, Characterization and Analysis) and U-Pb SHRIMP II facility at the John de Laeter Centre for Geochronology. Comments from John Geissman and an anonymous reviewer improved the quality of the paper.

References

Alvey, A. D. (2009), Using crustal thickness and continental lithosphere thinning factors from gravity inversion to refine plate reconstruction models for the Arctic and North Atlantic, Ph.D. thesis, Univ. of Liverpool, U. K., 189 pp.

Brabers, V. A. M., F. Walz, and H. Kronmüller (1998), Impurity effects upon the Verwey transition in magnetite, *Phys. Rev. B*, *58*(21), 14,163–14,166, doi:10.1103/PhysRevB.58.14163.

Brandt, D., M. Ernesto, A. C. Rocha-Campos, and P. R. dos Santos (2009), Paleomagnetism of the Santa Fé Group, central Brazil: Implications for the Late Paleozoic apparent polar wander path for South America, *J. Geophys. Res.*, *114*, B02101, doi:10.1029/2008JB005735.

Carvallo, C., A. R. Muxworthy, and D. J. Dunlop (2006), First-order reversal curve (FORC) diagrams of magnetic mixtures: Micromagnetic models and measurements, *Phys. Earth Planet. Inter.*, *154*(3–4), 308–322, doi:10.1016/j.pepi.2005.06.017.

Cogné, J. P. (2003), PaleoMac: A Macintosh (TM) application for treating paleomagnetic data and making plate reconstructions, *Geochem. Geophys. Geosyst.*, *4*(1), 1007, doi:10.1029/2001GC000227.

Dalziel, I. W. D., and A. M. Grunow (1992), Late Gondwanide tectonic rotations within Gondwanaland, *Tectonics*, *11*, 603–606, doi:10.1029/91TC02365.

Domeier, M., R. Van der Voo, R. N. Tomezzoli, T. H. Torsvik, H. Vizan, A. Dominguez, and J. Kirshner (2009), Alternative Pangea reconstructions: A Matter of flawed data? Implications of a new Early Triassic paleopole from Argentina, *Eos Trans. AGU*, *90*(22), Jt. Assem. Suppl., Abstract GP11E-05.

Dunlop, D. J., and Ö. Özdemir (1997), *Rock Magnetism: Fundamentals and Frontiers*, 596 pp., Cambridge Univ. Press, Cambridge, U. K., doi:10.1017/CBO9780511612794.

Fisher, R. A. (1953), Dispersion on a sphere, *Proc. R. Soc. London, Ser. A*, *217*, 295–305, doi:10.1098/rspa.1953.0064.

Forsythe, R. (1982), The Late Paleozoic to Early Mesozoic evolution of Southern South America: A plate tectonic interpretation, *J. Geol. Soc.*, *139*, 671–682, doi:10.1144/gsjgs.139.6.0671.

Geuna, S., and L. D. Escosteguy (2004), Paleomagnetism of the Upper Carboniferous–Lower Permian transition from Paganzo basin, Argentina, *Geophys. J. Int.*, *157*, 1071–1089, doi:10.1111/j.1365-246X.2004.02229.x.

Gilder, S., S. Rousse, D. Farber, B. McNulty, T. Sempere, V. Torres, and O. Palacios (2003), Post–middle Oligocene origin of paleomagnetic rotations in Upper Permian to Lower Jurassic rocks from northern and southern Peru, *Earth Planet. Sci. Lett.*, *210*(1–2), 233–248, doi:10.1016/S0012-821X(03)00102-X.

Gradstein, F. M., J. G. Ogg, and A. G. Smith (2004), *A Geologic Time Scale 2004*, 610 pp., Cambridge Univ. Press, Cambridge, U. K.

Halls, H. C. (1978), The use of converging remagnetization circles in palaeomagnetism, *Phys. Earth Planet. Inter.*, *16*(1), 1–11, doi:10.1016/0031-9201(78)90095-X.

Harrison, C. G. A. (2009), Latitudinal signature of Earth's magnetic field variation over the last 5 million years, *Geochem. Geophys. Geosyst.*, *10*, Q02012, doi:10.1029/2008GC002298.

Heredia, N., L. R. Rodríguez Fernández, G. Gallastegui, P. Busquets, and F. Colombo (2002), Geological setting of the Argentine Frontal Cordillera in the flat-slab segment (30°00′–31°30′S latitude), *J. South Am. Earth Sci.*, *15*, 79–99, doi:10.1016/S0895-9811(02)00007-X.

Irving, E. (1977), Drift of the major continental blocks since the Devonian, *Nature*, *270*, 304–309, doi:10.1038/270304a0.

Irving, E. (2004), The case for Pangea B, and the Intra-Pangean megashear, in *Timescales of the Paleomagnetic Field*, *Geophys. Monogr. Ser.*, vol. 145, edited by James E. T. Channell et al., pp. 13–27, AGU, Washington, D. C.

Jesinkey, C., R. D. Forsythe, C. Mpodozis, and J. Davidson (1987), Concordant Late Paleozoic paleomagnetizations from the Atacama Desert: Implications for tectonic models of the Chilean Andes, *Earth Planet. Sci. Lett.*, *85*(4), 461–472, doi:10.1016/0012-821X(87)90141-5.

Kay, S. M., V. A. Ramos, C. Mpodozis, and P. Sruoga (1989), Late Paleozoic to Jurassic silicic magmatism at the Gondwana margin: Analogy to middle Proterozoic in North America?, *Geology*, *17*, 324–328, doi:10.1130/0091-7613(1989)017<0324:LPTJSM>2.3.CO;2.

Kirschvink, J. L. (1980), The least squares line and plane and the analysis of paleomagnetic data, *Geophys. J. R. Astron. Soc.*, *62*, 699–718.

Kleiman, L. E., and M. S. Japas (2009), The Choiyoi volcanic province at 34°S–36°S (San Rafael, Mendoza, Argentina): Implications for the Late Palaeozoic evolution of the southwestern margin of Gondwana, *Tectonophysics*, *473*, 283–299, doi:10.1016/j.tecto.2009.02.046.

Lewis, T., and N. I. Fisher (1982), Graphical methods for investigating the fit of a Fisher distribution for spherical data, *Geophys. J. R. Astron. Soc.*, *69*, 1–13.

Libarkin, J., R. Butler, D. Richards, and T. Sempere (1998), Tertiary remagnetization of Paleozoic rocks from the Eastern Cordillera and sub-Andean belt of Bolivia, *J. Geophys. Res.*, *103*, 30,417–30,429, doi:10.1029/98JB02848.

Lipman, P. W. (1997), Subsidence of ash-flow calderas: Relation to caldera size and magma-chamber geometry, *Bull. Volcanol.*, *59*, 198–218, doi:10.1007/s004450050186.

Llambías, E. J. (1973), Las ignimbritas de la Sierra de Lihue-Calel, provincia de La Pampa, *Actas Congr. Geol. Argent.*, *4*, 55–67.

Llambías, E. J., and A. M. Sato (1995), El Batolito de Colangüil: Transición entre orogénesis y anorogénesis, *Asoc. Geol. Argent. Rev.*, *50*(1–4), 111–131.

Llambías, E. J., L. E. Kleiman, and J. A. Salvarredi (1993), Magmatismo gondwánico de Mendoza, in *Geología y Recursos Naturales de Mendoza*, edited by V. A. Ramos, pp. 53–64, La Comisión, Buenos Aires.

Llambías, E. J., S. Quenardelle, and T. Montenegro (2003), The Choiyoi Group from central Argentina: A subalkaline transitional to alkaline association in the craton adjacent to the active margin of Gondwana continent, *J. South Am. Earth Sci.*, *16*, 243–257, doi:10.1016/S0895-9811(03)00070-1.

Lock, B. E. (1980), Flat-plate subduction and the Cape Fold Belt of South Africa, *Geology*, *8*, 35–39, doi:10.1130/0091-7613(1980)8<35:FSATCF>2.0.CO;2.

Ludwig, K. R. (2003), User's manual for Isoplot/Ex, version 3.0: A geochronological toolkit for Microsoft Excel, *Spec. Publ. 4*, Berkeley Geochron. Cent., Berkeley, Calif.

Martin, M. W., J. R. Clavero, and C. M. Mpodozis (1999), Late Paleozoic to Early Jurassic tectonic development of the high Andean Principal Cordillera, El Indio Region, Chile (29–30°S), *J. South Am. Earth Sci.*, *12*, 33–49, doi:10.1016/S0895-9811(99)00003-6.

McFadden, P. L. (1980), Testing a palaeomagnetic study for the averaging of secular variation, *Geophys. J. R. Astron. Soc.*, *61*, 183–192.

McFadden, P. L., and M. W. McElhinny (1988), The combined analysis of remagnetization circles and direct observations in paleomagnetism, *Earth Planet. Sci. Lett.*, *87*, 161–172, doi:10.1016/0012-821X(88)90072-6.

Moskowitz, B. M., M. Jackson, and C. Kissel (1998), Low-temperature magnetic behavior of titanomagnetites, *Earth Planet. Sci. Lett.*, *157*, 141–149, doi:10.1016/S0012-821X(98)00033-8.

Mpodozis, C., and S. M. Kay (1992), Late Paleozoic to Triassic evolution of the Gondwana margin: Evidence from Chilean Frontal Cordilleran batholiths (28° to 31° S), *Geol. Soc. Am. Bull.*, *104*, 999–1014, doi:10.1130/0016-7606(1992)104<0999:LPTTEO>2.3.CO;2.

Muttoni, G., D. V. Kent, and J. E. T. Channell (1996), Evolution of Pangea: Paleomagnetic constraints from the Southern Alps, Italy, *Earth Planet. Sci. Lett.*, *140*, 97–112, doi:10.1016/0012-821X(96)00038-6.

Muttoni, G., D. V. Kent, E. Garzanti, P. Brack, N. Abrahamsen, and M. Gaetani (2003), Early Permian Pangea 'B' to Late Permian Pangea 'A', *Earth Planet. Sci. Lett.*, *215*(3–4), 379–394, doi:10.1016/S0012-821X(03)00452-7.

Muxworthy, A. R., and E. McClelland (2000), Review of the low-temperature magnetic properties of magnetite from a rock magnetic perspective, *Geophys. J. Int.*, *140*, 101–114, doi:10.1046/j.1365-246x.2000.00999.x.

Nomade, S., K. B. Knight, E. Beutel, P. R. Renne, C. Verati, G. Feraud, A. Marzoli, N. Youbi, and H. Bertrand (2007), Chronology of the Central Atlantic Magmatic Province: Implications for the Central Atlantic rifting processes and the Triassic-Jurassic biotic crisis, *Palaeogeogr. Palaeoclimatol. Palaeoecol.*, *244*, 326–344, doi:10.1016/j.palaeo.2006.06.034.

Opdyke, N. D., J. Roberts, J. Claoue-Long, E. Irving, and P. J. Jones (2000), Base of the Kiaman: Its definition and global stratigraphic significance, *Geol. Soc. Am. Bull.*, *112*, 1315–1341, doi:10.1130/0016-7606(2000)112<1315:BOTKID>2.0.CO;2.

Özdemir, Ö., D. J. Dunlop, and B. M. Moskowitz (1993), The effect of oxidation on the Verwey transition in magnetite, *Geophys. Res. Lett.*, *20*(16), 1671–1674, doi:10.1029/93GL01483.

Özdemir, Ö., D. J. Dunlop, and T. S. Berquó (2008), Morin transition in hematite: Size dependence and thermal hysteresis, Morin transition in hematite: Size dependence and thermal hysteresis, *Geochem. Geophys. Geosyst.*, *9*, Q10Z01, doi:10.1029/2008GC002110.

Pankhurst, R. J., C. W. Rapela, C. M. Fanning, and M. Márquez (2006), Gondwanide continental collision and the origin of Patagonia, *Earth Sci. Rev.*, *76*, 235–257, doi:10.1016/j.earscirev.2006.02.001.

Quenardelle, S. M., and E. J. Llambías (1997), Las riolitas de Sierra Chica (37°S, 65°O): Un centro eruptivo gondwánico en el bloque del Chadileuvú, provincia de La Pampa, Argentina, *Asoc. Geol. Argent. Rev.*, *52*(4), 549–558.

Rakotosolofo, N. A., J. A. Tait, V. Carlotto, and J. Cárdenas (2006), Paleomagnetic results from the Early Permian Copacabana Group, southern Peru: Implication for Pangea palaeogeography, *Tectonophysics*, *413*(3–4), 287–299, doi:10.1016/j.tecto.2005.10.043.

Ramos, V. A. (2008), Patagonia: A Paleozoic continent adrift?, *J. South Am. Earth Sci.*, *26*, 235–251, doi:10.1016/j.jsames.2008.06.002.

Rapalini, A. E. (1998), Syntectonic magnetization of the mid-Paleozoic Sierra Grande formation: Further constraints for the tectonic evolution of Patagonia, *J. Geol. Soc.*, *155*, 105–114, doi:10.1144/gsjgs.155.1.0105.

Rapalini, A. E., and R. Astini (2005), La remagnetización Sanrafaélica de la Precordillera en el Pérmico: Nuevas evidencias, *Asoc. Geol. Argent. Rev.*, *60*(2), 290–300.

Rapalini, A. E., and C. A. Cingolani (2004), First Late Ordovician paleomagnetic pole for the Cuyania (Precordillera) terrane of Western Argentina: A microcontinent or a Laurentian Plateau, *Gondwana Res.*, *7*(4), 1089–1104, doi:10.1016/S1342-937X(05)71086-8.

Rapalini, A. E., and L. Sánchez Bettucci (2008), Widespread remagnetization of late Proterozoic sedimentary units of Uruguay and the apparent polar wander path for the Rio de La Plata Craton, *Geophys. J. Int.*, *174*, 55–74, doi:10.1111/j.1365-246X.2008.03771.x.

Rapalini, A. E., and D. H. Tarling (1993), Multiple magnetizations in the Cambrian-Ordovician carbonate platform of the Argentine Precordillera and their tectonic implications, *Tectonophysics*, *227*, 49–62, doi:10.1016/0040-1951(93)90086-Y.

Rapalini, A. E., and J. F. Vilas (1991), Tectonic rotations in the Late Palaeozoic continental margin of southern South America determined and dated by palaeomagnetism, *Geophys. J. Int.*, *107*, 333–351, doi:10.1111/j.1365-246X.1991.tb00829.x.

Rapalini, A. E., J. F. Vilas, M. L. Bobbio, and D. A. Valencio (1989), Geodynamic interpretations from paleomagnetic data of Late Paleozoic rocks in the Southern Andes, in *Deep Structure and Past Kinematics of Accreted Terranes* (IUGG vol. 5), *Geophys. Monogr. Ser.*, edited by J. W. Hillhouse, vol. 50, 41–57, AGU, Washington D. C.

Rapalini, A. E., S. Fazzito, and D. Orué (2006), A new Late Permian paleomagnetic pole for stable South America: The Independencia group, eastern Paraguay, *Earth Planets Space*, *58*, 1247–1253.

Rapela, C. W., R. J. Pankhurst, E. J. Llambías, C. Labudía, and A. Artabe (1996), "Gondwana" magmatism of Patagonia: Inner cordilleran calc-alkaline batholiths and bimodal volcanic provinces, paper presented at 3rd International Symposium on Andean Geodynamics, Inst. de Rech. pour le Dev., St. Malo, France.

Roberts, A. P., C. R. Pike, and K. L. Verosub (2000), First-order reversal curve diagrams: A new tool for characterizing the magnetic properties of natural samples, *J. Geophys. Res.*, *105*(B12), 28,461–28,475, doi:10.1029/2000JB900326.

Somoza, R., and C. B. Zaffarana (2008), Mid-Cretaceous polar standstill of South America, motion of the Atlantic hotspots and the birth of the Andean cordillera, *Earth Planet. Sci. Lett.*, *271*, 267–277, doi:10.1016/j.epsl.2008.04.004.

Sruoga, P., and E. J. Llambías (1992), Permo-Triassic leucorhyolitic ignimbrites at Sierra de Lihue Calel, La Pampa Province, Argentina, *J. South Am. Earth Sci.*, *5*(2), 141–152, doi:10.1016/0895-9811(92)90035-W.

Tauxe, L. (2010), *Essentials of Paleomagnetism*, 489 pp., Univ. of Calif. Press, Berkeley, Calif.

Tauxe, L., and G. S. Watson (1994), The fold test: An eigen analysis approach, *Earth Planet. Sci. Lett.*, *122*, 331–341, doi:10.1016/0012-821X(94)90006-X.

Tauxe, L., N. Kylstra, and C. Constable (1991), Bootstrap statistics for paleomagnetic data, *J. Geophys. Res.*, *96*, 11,723–11,740, doi:10.1029/91JB00572.

Terrizzano, C. M. (2005), Nuevos estudios paleomagnéticos en el Bloque de San Rafael, provincia de Mendoza, Dep. de Geol., Master thesis, 118 pp., Univ. de Buenos Aires, Buenos.

Tickyj, H., L. V. Dimieri, E. J. Llambías, and A. M. Sato (1997), Cerro de Los Viejos (38° 28′ S–64° 26′ O): Cizallamiento dúctil en el sudeste de La Pampa, *Asoc. Geol. Argent. Rev.*, *52*(3), 311–321.

Tomezzoli, R. N. (2001), Further paleomagnetic results from the Sierras Australes fold and thrust belt, Argentina, *Geophys. J. Int.*, *147*, 356–366, doi:10.1046/j.0956-540x.2001.01536.x.

Tomezzoli, R. N. (2009), The apparent polar wander path for South America during the Permian-Triassic, *Gondwana Res.*, *15*(2), 209–215, doi:10.1016/j.gr.2008.10.005.

Tomezzoli, R. N., and J. F. Vilas (1999), Paleomagnetic constraints on age of deformation of the Sierras Australes thrust and fold belt, *Geophys. J. Int.*, *138*, 857–870, doi:10.1046/j.1365-246x.1999.00914.x.

Tomezzoli, R. N., R. Melchor, and W. D. MacDonald (2006), Tectonic implications of post-folding Permian magnetizations, Carapacha basin, Argentina, *Earth Planets Space*, *58*, 1235–1246.

Tomezzoli, R. N., T. Saint Pierre, and C. Valenzuela (2008), New palaeomagnetic results from Late Paleozoic volcanic units along the western Gondwana margin in La Pampa, Argentina, *Earth Planets Space*, *60*, 1–7.

Torcq, F., J. Besse, D. Vaslet, J. Marcoux, L. E. Ricou, M. Halawani, and M. Basahel (1997), Paleomagnetic results from Saudi Arabia and the Permo-Triassic Pangea configuration, *Earth Planet. Sci. Lett.*, *148*, 553–567, doi:10.1016/S0012-821X(97)00047-2.

Torsvik, T. H., R. D. Muller, R. Van der Voo, B. Steinberger, and C. Gaina (2008), Global plate motion frames: Toward a unified model, *Rev. Geophys.*, *46*, RG3004, doi:10.1029/2007RG000227.

Torsvik, T. H., S. Rousse, C. Labails, and M. Smethurst (2009), A new scheme for the opening of the South Atlantic Ocean and the dissection of an Aptian salt basin, *Geophys. J. Int.*, *177*(3), 1315–1333.

Trouw, R. A. J., and M. J. De Wit (1999), Relation between the Gondwanide Orogen and contemporaneous intracratonic deformation, *J. Afr. Earth Sci.*, *28*(1), 203–213, doi:10.1016/S0899-5362(99)00024-X.

Van der Voo, R. (1990), The reliability of paleomagnetic data, *Tectonophysics*, *184*(1), 1–9, doi:10.1016/0040-1951(90)90116-P.

Veldkamp, J., F. G. Mulder, and J. D. A. Zijderveld (1971), Palaeomagnetism of Suriname dolerites, *Phys. Earth Planet. Inter.*, *4*(5), 370–380, doi:10.1016/0031-9201(71)90020-3.

Visser, J. N. J., and H. E. Praekelt (1998), Late Palaeozoic crustal block rotations within the Gondwana sector of Pangea, *Tectonophysics*, *287*, 201–212, doi:10.1016/S0040-1951(98)80069-3.

Vizan, H., R. Ixer, P. Turner, J. M. Cortes, and G. Cladera (2004), Paleomagnetism of Upper Triassic rocks in the Los Colorados hill section, Mendoza province, Argentina, *J. South Am. Earth Sci.*, *18*(1), 41–59, doi:10.1016/j.jsames.2004.08.008.

Zijderveld, J. D. A. (1967), A.C. demagnetization of rocks: Analysis of results, in *Methods in Paleomagnetism*, edited by D. W. Collinson, K. M. Creer, and S. K. Runcorn, pp. 254–286, Elsevier, Amsterdam.